Geological Society, London, Special Publications

Tertiary cooling and exhumation history in the Maramures area (internal eastern Carpathians, northern Romania): thermochronology and structural data

H. R. Gröger, B. Fügenschuh, M. Tischler, S. M. Schmid and J. P. T. Foeken

Geological Society, London, Special Publications 2008; v. 298; p. 169-195
doi:10.1144/SP298.9

Notes

Tertiary cooling and exhumation history in the Maramures area (internal eastern Carpathians, northern Romania): thermochronology and structural data

H. R. GRÖGER[1,2], B. FÜGENSCHUH[3], M. TISCHLER[1], S. M. SCHMID[1] & J. P. T. FOEKEN[4]

[1]*Geologisch Paläontologisches Institut, Universität Basel, Bernoullistrasse 32, 4056 Basel, Switzerland*

[2]*Present address: Statoil ASA, Forusbeen 50, 4035 Stavanger, Norway (e-mail: heigr@statoilhydro.com)*

[3]*Institut für Geologie und Paläontologie, Universität Innsbruck, Innrain 52, Bruno Sander Haus, 6020 Innsbruck, Austria*

[4]*Scottish Universities Environmental Research Centre (SUERC), Rankine Avenue, Scottish Enterprise Technology Park, East Kilbride, G75 0QF, Scotland*

Abstract: The Tertiary kinematic history of the Maramures area is constrained by integrating thermochronological (fission track and (U–Th)/He analysis) data with field-based structural investigations. This study focuses on the tectonic evolution of the northern rim of the Tisza–Dacia block during collision with the European margin. Cretaceous nappe stacking, related metamorphism as well as Late Cretaceous exhumation are evidenced by zircon fission track data. Subsequent Palaeogene to Early Miocene sedimentation led to burial heating and annealing of fission tracks in apatite. Final tectonic uplift was initiated during the convergence of Tisza–Dacia with the European margin, associated with transpressional deformation (16 to 12 Ma). This led to Mid-Miocene exhumation, recorded by apatite fission track cooling ages in the western part of the study area. Transtension between 12 and 10 Ma caused brittle deformation along E–W trending strike-slip faults and SW–NE trending normal faults, delimiting blocks that were tilted towards the SW. This fragmentation of the crust led to enhanced exhumation at rates of 1 mm/a in the central part of the study area, as is documented by Middle to Late Miocene cooling ages (13 to 7 Ma). The outside estimate for the total amount of exhumation since Middle Miocene times is 7 km.

This study addresses the cooling and exhumation history of basement units (Rodna horst and Preluca massif) in northern Romania (Maramures) by combining thermochronological analyses with structural field investigations. The study area is located in the NE prolongation of the Mid-Hungarian fault zone (Csontos & Nagymarosy 1998; Csontos & Vörös 2004), separating the ALCAPA and Tisza–Dacia mega-units (Fig. 1). This crustal-scale boundary plays a key role during the final emplacement of these two crustal-scale blocks (ALCAPA and Tisza–Dacia) in the Carpathian embayment during the Tertiary (Csontos & Nagymarosy 1998). Since the Mid-Hungarian fault zone is largely covered by Neogene sediments of the Pannonian basin, our study area represents one of the very few places where structures related to this important tectonic lineament can be studied in outcrop (Tischler *et al.* 2006).

Invasion of the ALCAPA and Tisza–Dacia blocks into the Carpathian embayment was triggered by a combination of lateral extrusion in the eastern Alps (Ratschbacher *et al.* 1991*a*, *b*) and retreat of the European lithospheric slab (e.g. Wortel & Spakman 2000; Sperner *et al.* 2005). Corner effects at the Moesian and Bohemian promontories led to opposed rotations of these continental blocks during their emplacement, well established by palaeomagnetic studies (e.g. Márton 2000; Márton & Fodor 1995, 2003; Márton *et al.* 2006). The Mid-Hungarian fault zone is of central importance, since it allows for differential movements between the ALCAPA and Tisza–Dacia blocks (Fodor *et al.* 1999; Csontos & Vörös 2004). Finally, soft collision of these blocks with the European continental margin resulted in the formation of the Miocene fold and thrust belt (Fig. 1; e.g. Royden 1988; Roure *et al.* 1993; Matenco & Bertotti 2000). A more detailed

From: SIEGESMUND, S., FÜGENSCHUH, B. & FROITZHEIM, N. (eds) *Tectonic Aspects of the Alpine-Dinaride-Carpathian System.* Geological Society, London, Special Publications, **298**, 169–195.
DOI: 10.1144/SP298.9 0305-8719/08/$15.00

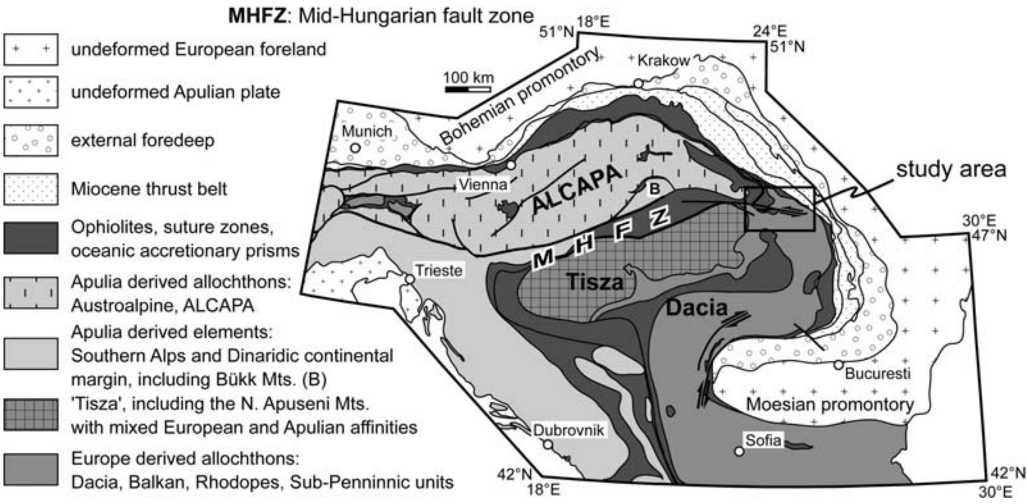

Fig. 1. Tectonic map of the Alpine–Carpathian–Pannonian area (simplified after Schmid *et al.* 2006). Three major continental blocks are located within the Carpathian embayment: ALCAPA, Tisza and Dacia. During emplacement in Tertiary times, a zone of repeated tectonic activity developed between ALCAPA and the previously consolidated Tisza–Dacia block: the Mid-Hungarian fault zone (MHFZ).

discussion of the Tertiary palaeogeographic and kinematic history of the ALCAPA and Tisza–Dacia blocks can be found in numerous earlier studies (e.g. Balla 1987; Royden & Baldi 1988; Săndulescu 1988; Csontos 1995; Csontos *et al.* 1992; Fodor *et al.* 1999; Fügenschuh and Schmid 2005).

The samples analysed in this study derive from pre-Mesozoic basement and the autochthonous sedimentary cover of the Tisza–Dacia block (Preluca massif, Rodna and Maramures Mountains, respectively) and from tectonic units that are part of an accretionary prism which is situated between the ALCAPA and Tisza–Dacia blocks, the so-called Pienides. According to a recent compilation of tectonic units by Schmid *et al.* (2006), the basement units are considered part of Dacia, but classically the Preluca massif, which is part of the Biharia nappe system, is attributed to Tisza (e.g. Haas & Péró 2004). We applied zircon fission track-, apatite fission track- and apatite (U–Th)/He thermochronological analyses. The combination of these methods constrains the thermal history of the samples in the temperature range between 300 °C and 40 °C, and is well suited to elucidate the thermal evolution in soft collisional regimes, which do not feature major exhumation and exposure of high grade metamorphic rocks (Royden 1993; Morley 2002).

Numerous other studies successfully addressed cooling and exhumation histories, either based on fission track analyses alone (e.g. Sobel & Dumitru 1997; Fügenschuh *et al.* 2000; Dunkl & Frisch 2002; Danišík *et al.* 2004; Fügenschuh & Schmid 2003, 2005) or on a combination of fission track and (U–Th)/He analyses (e.g. Foeken *et al.* 2003; Reiners *et al.* 2003; Persano *et al.* 2005; Stöckli 2005 and references therein). Within our working area, some apatite fission track data are already available from the work of Sanders (1998) and Sanders *et al.* 1999, who addressed the interplay between tectonics and erosion in the southern and eastern Carpathians and the Apuseni Mountains.

All chronostratigraphic ages will be given after Gradstein *et al.* (2004). Paratethys stages were correlated with Mediterranean stages according to Steininger & Wessely (2000).

Geological setting

The Precambrian to Palaeozoic basement units of the east Carpathians (so-called Bucovinian nappe stack of the Dacia block) mainly consist of metasediments and subordinately orthogneiss (Kräutner 1991; Voda & Balintoni 1994). The Alpine-age Bucovinian nappe stack consists, from bottom to top, of the Infrabucovinian, Subbucovinian and Bucovinian nappes, occasionally separated by Permian to Lower Cretaceous sediments (Săndulescu *et al.* 1981). Along most parts of the east Carpathians, late Early Cretaceous nappe stacking is generally considered to have taken place under sub-greenschist facies metamorphic conditions. In the so-called Rodna horst (Fig. 2), a part of the Bucovinian nappe stack located

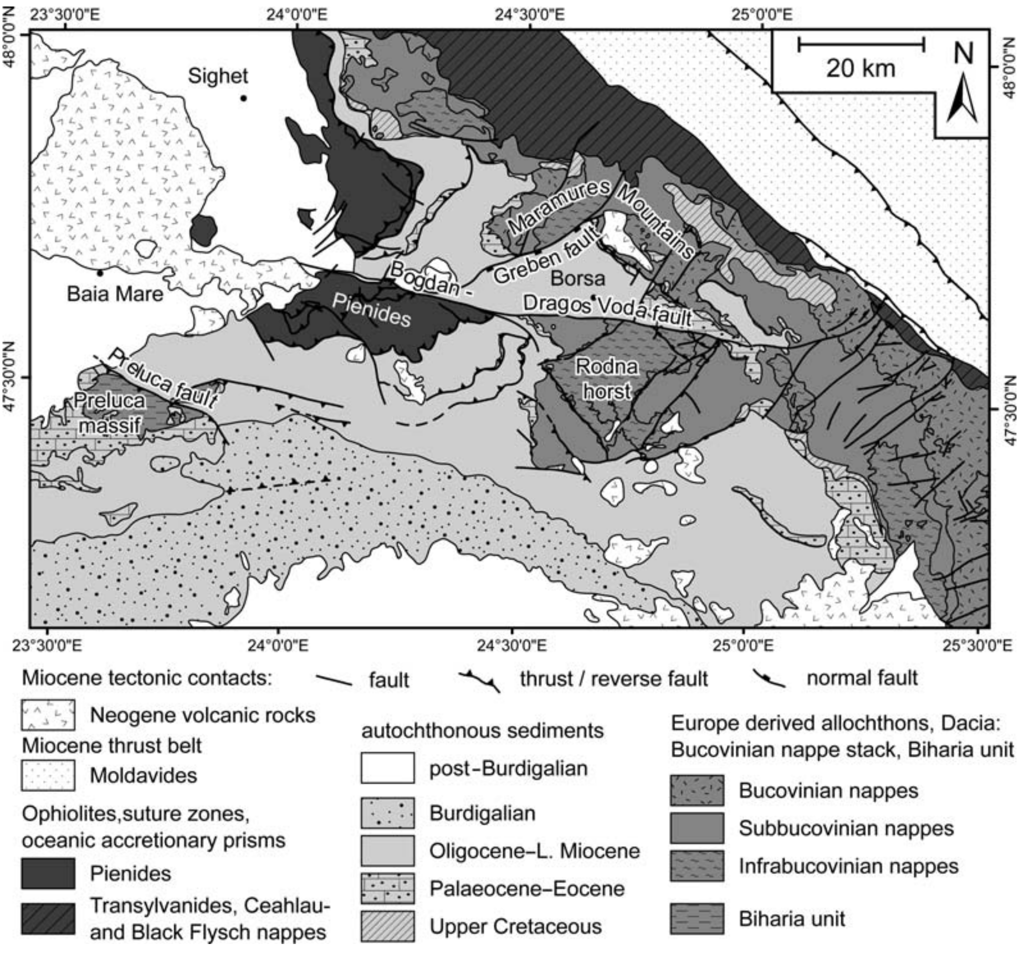

Fig. 2. Tectonic map of the study area. The Pienides, consisting of non-metamorphic flysch nappes, were emplaced in Early Burdigalian times (20.5 to 18.5 Ma, Tischler *et al.* 2006). Middle to Late Miocene brittle tectonics (16 to 10 Ma) led to the exhumation of the Rodna horst and the Preluca massif (Tischler *et al.* 2006). The most important Middle to Late Miocene structures are the Preluca fault, the Greben fault and the Bogdan–Dragos–Voda fault. To the west, the Bogdan–Voda fault is sealed by Neogene volcanic rocks. The map is compiled after Giusca & Radulescu (1967), Raileanu & Radulescu (1967), Raileanu & Saulea (1968), Ianovici & Dessila-Codarcea (1968), Ianovici & Radulescu (1968), Ianovici *et al.* (1968), Kräutner *et al.* (1978, 1982, 1983, 1989), Borcos *et al.* (1980), Dicea *et al.* (1980), Sandulescu (1980), Sandulescu & Russo-Sandulescu (1981), Sandulescu *et al.* (1981), Rusu *et al.* (1983), Sandulescu *et al.* (1991) and Aroldi (2001).

internally of the main east Carpathian chain, greenschist facies conditions during this event were postulated by Balintoni *et al.* (1997). The Preluca massif, consisting of metasediments (Rusu *et al.* 1983), is part of the Biharia nappe system of the North Apuseni Mountains. However, in contrast to most authors (e.g. Haas & Péró 2004), the Biharia nappe system was correlated with the Bucovinian nappe system (i.e. considered as part of Dacia) by Schmid *et al.* (2006), based on a re-interpretation of geophysical data from the Transylvanian basin. In any case, Tisza and Dacia became amalgamated during the Cretaceous and formed a consolidated Tisza–Dacia block ever since Early Tertiary times (Csontos 1995; Csontos & Vörös 2004).

Latest Early Cretaceous juxtaposition of the Bucovinian nappe stack against the Ceahlau and Black Flysch units (Săndulescu 1982) was followed by exhumation and erosion, leading to the sedimentation of the Late Cretaceous post-tectonic cover (Ianovici *et al.* 1968; Săndulescu 1994). Exhumation which followed the juxtaposition of the entire Alpine nappe pile against the internal

Moldavides (Săndulescu 1982) occurred during the latest Cretaceous (Săndulescu 1994) and led to erosion of large parts of these Upper Cretaceous cover units.

The deposition of a second stack of post-tectonic sediments during the Tertiary led to renewed burial. While the sedimentation already started in Palaeocene times in the Preluca massif (Rusu *et al.* 1983), non-deposition and/or erosion continues in the area of the Bucovinian nappe stack, as is indicated by a Palaeocene hiatus. Eocene conglomerates (Ypresian?, Kräutner *et al.* 1983) are the oldest Tertiary strata preserved on the previously exhumed Bucovinian nappe stack which they stratigraphically directly overlie except for a few places where the Late Cretaceous basins remained preserved (Fig. 2). Late Eocene (Late Lutetian–Priabonian) sedimentation is characterized by a general deepening of the depositional environment towards the NW. While platform carbonates indicating shallow water depths are found in large parts of the study area (main east Carpathian Chain and Rodna horst: Kräutner *et al.* 1978, 1982, 1983, 1989; Preluca massif: Rusu *et al.* 1983; de Broucker *et al.* 1998), sandy marls and marls dominate west of the Greben fault (Fig. 2; Săndulescu *et al.* 1991). Oligocene sediments overlying the basement units of the Rodna horst in direct stratigraphic contact document the Eocene palaeorelief (Kräutner *et al.* 1982).

Early Oligocene to Early Miocene (Aquitanian) sedimentation is dominated by siliciclastic turbidites, which show an overall coarsening-upward trend (Dicea *et al.* 1980; Săndulescu *et al.* 1991), thought to reflect the juxtaposition of ALCAPA and Tisza–Dacia (Tischler *et al.* 2008). A Burdigalian clastic wedge (Hida beds) testifies the overthrusting of the Pienides (Ciulavu *et al.* 2002), i.e. thrusting of ALCAPA onto Tisza–Dacia. The Pienides mainly consist of Eocene to Oligocene non-metamorphic flysch units (Aroldi 2001), which additionally contain phacoids of Pieniny-Klippen-type material embedded in Eocene flysch (Săndulescu 1980; Săndulescu *et al.* 1993).

Post-Burdigalian sedimentation starts with the deposition of the Middle Miocene (Badenian) Dej Tuff (Mason *et al.* 1998). Subduction-related calc-alkaline magmatism started during Middle Miocene times (13.5 Ma, Pécskay *et al.* 1995). Magmatic activity led to the formation of a linear volcanic chain along the inner side of the east Carpathians, with a general trend of decreasing ages towards the SE.

The most obvious structure in the study area is the E–W striking, predominantly left-lateral Bogdan–Dragos–Voda fault system (Tischler *et al.* 2006). The Bogdan–Voda fault to the west offsets the Palaeogene to Early Miocene cover of Tisza–Dacia, as well as the nappe pile of the Pienides. It is essentially sealed by Mid-Miocene volcanic rocks (Fig. 2). The Dragos–Voda fault delimits the Rodna horst to the north.

Methods

Fission track analysis: methodology and analytical procedure

For an overview of the methodology and applications of fission track (FT) analysis, the reader is referred to Wagner and van den Haute (1992), Andriessen (1995), Gallagher *et al.* (1998) and Reiners & Ehlers (2005). Regarding the fission track partial annealing zones, we used the temperature brackets given by Gleadow & Duddy (1981) and Green *et al.* (1989) for apatite (APAZ, 60 to 120 °C) and Hurford (1986) for zircon (ZPAZ, 190 to 290 °C), respectively.

After conventional crushing, sieving, magnetic and heavy liquid separation, apatite grains were mounted in epoxy resin, polished and etched for 40 seconds at room temperature in 6.5% HNO_3. Zircon grains were mounted in PFA® Teflon, polished and etched for 12 to 24 hours in a NaOH/KOH eutectic melt at about 225 °C. Irradiation was carried out at the High Flux Australian Reactor (HIFAR) with neutron fluxes monitored in CN5 for apatite and CN1 for zircon. All samples were analysed using the external detector method (Gleadow 1981) with muscovite as an external detector. Muscovite was etched for 40 minutes at room temperature in 40% HF.

Fission tracks were counted on a Zeiss® microscope with a computer-controlled scanning stage ('Langstage', Dumitru 1993) at magnifications of ×1250 for apatite and ×1600 for zircon (dry). Unless mentioned otherwise, all ages given are central ages (Galbraith & Laslett 1993). Ages were calculated using the zeta calibration method (Hurford & Green 1983) with a ξ value of 355.96 ± 9.39 (Durango standard, CN5) for apatite and 141.40 ± 6.33 (Fish Canyon tuff standard, CN1) for zircon. Calculations were done with the aid of the Windows software TrackKey (Dunkl 2002). For separation of subpopulations (i.e. the youngest population in partially annealed samples), the Windows software PopShare was used (Dunkl & Székely 2002).

Lengths of confined horizontal tracks in apatite were measured at ×1250 magnification. Track length distributions of confined horizontal tracks are diagnostic for different thermal histories (Crowley 1985; Gleadow *et al.* 1986*a, b*; Galbraith & Laslett 1993) and allow for thermal modelling. Thermal modelling of fission track parameters was carried out with the program AFTSolve (Ketcham *et al.* 2000) with the annealing model of Laslett *et al.* (1987).

Apart from temperature, chemical composition is known to have an effect on the annealing behaviour (Green *et al.* 1985, 1986; Crowley & Cameron 1987; ÒSullivan & Parrish 1995; Siddall & Hurford 1998). Thus, the long axis of etch pits on the polished surface (referred to as Dpar, Burtner *et al.* 1994) was measured (magnification $\times 2000$) as an indicator of the annealing behaviour of apatite.

Apatite (U–Th)/He dating: methodology and analytical procedure

Apatite (U–Th)/He dating records the cooling of a sample between 80 and 40 °C (Wolf *et al.* 1998; Ehlers & Farley 2003 and references therein) and is complementary to apatite FT when reconstructing the latest exhumation stages. Apatite (U–Th)/He analyses were conducted on four samples: two from the Rodna horst and two from the Preluca massif. Suitability of samples for (U–Th)/He dating was mainly governed by sample quality (inclusions) and grain morphology. Between one to four apatite grains for each sample were hand-picked in ethanol at $\times 218$ magnification using a binocular microscope. While the frosted nature of the apatite grains made the identification of inclusion-free grains difficult, small zircon inclusions were only observed in one replicate of sample P4 (II). To minimize grain size variation effects (Farley 2000), grains of similar radius were selected for each aliquot. ^{4}He, U and Th analyses were conducted following the procedures of Balestrieri *et al.* (2005). The total analytical uncertainty of He ages of each aliquot is approximately $\pm 10\%$ (2σ), governed largely by uncertainty in blank corrections and spike concentrations. Correction for He recoil loss was made using procedures described in Farley (2002). Analyses of a Durango apatite standard aliquot (two grains) yield 33.1 $\pm$ 0.7 Ma, which is indistinguishable from mean Durango ages measured at SUERC (32.8 $\pm$ 1.3 Ma, Foeken *et al.* 2006) and reported Durango ages (e.g. 32.1 $\pm$ 1.7 Ma, House *et al.* 2000).

Results of kinematic analyses

In the following, only a summary of the Middle to Late Miocene tectonic evolution of the study area will be given (see Tischler *et al.* 2006 for a detailed discussion). Two stages dominated by brittle sinistral strike-slip deformation are documented in the study area: Middle Miocene transpression (Fig. 3a), followed by Middle to Late Miocene transtension (Fig. 3b). During both stages, shortening remained NE–SW oriented. The most obvious structures related to these stages are the E–W striking Bogdan–Voda fault (BVF) and the Dragos–Voda fault (DVF). The left lateral activity of the Bogdan–Voda fault is already apparent in map view, as evidenced by the 25 km sinistral offset of the Burdigalian-age thrust contact of the Pienides (Fig. 3).

During the transpressional stage, the Bogdan–Voda fault was active as a sinistrally transpressive fault, terminating eastwards in a thrust splay geometry (Fig. 3a). Other major structures attributed to this first transpressional stage are NW–SE striking reverse faults (e.g. a back-thrust NE of Borsa), the Preluca fault (PF), as well as very open NW–SE to WNW–ESE striking folds.

During the later transtensional stage (Fig. 3b), the Bogdan–Voda and Dragos–Voda faults both acted together as one single continuous fault. Sinistral offset along the so-called Bogdan–Dragos–Voda fault system (Tischler *et al.* 2006) diminishes eastwards and terminates in an extensional horsetail splay geometry. Additional features attributed to this second stage are SW–NE-striking normal faults, such as the Greben fault and numerous faults within the Rodna horst (Fig. 3b).

Results of the thermochronological analysis

Sampling approach

All sample localities are depicted in Figure 4. The Preluca massif is covered by four samples (P1, P2, P3, P4) while three samples are from an immediately adjacent smaller basement body located further to the NE (P5, P6, P7). The Maramures Mountains further to the NE have been sampled along two orthogonal profiles, yielding a total of 10 samples. One profile is orogen-perpendicular (samples M01, M02, M03, M04, M05); the other one crosses the Greben fault and the horsetail splay of the Bogdan–Dragos–Voda fault (samples M06, M08, M07, M09, M13, M14). In the area of the Rodna horst, located S of the Dragos–Voda fault, four vertical profiles have been sampled, each of them within a distinct fault-bounded block. Each profile comprises five to six samples (see groups of samples listed under R1, R2, R3 and R4 in Fig. 4). Additional samples have been collected within the central block of the Rodna horst and adjacent to the Dragos–Voda fault (sample group R5). The basement samples comprise mainly paragneisses and rarely orthogneiss.

A last group of samples has been taken from sedimentary formations. The samples S2, S4 and

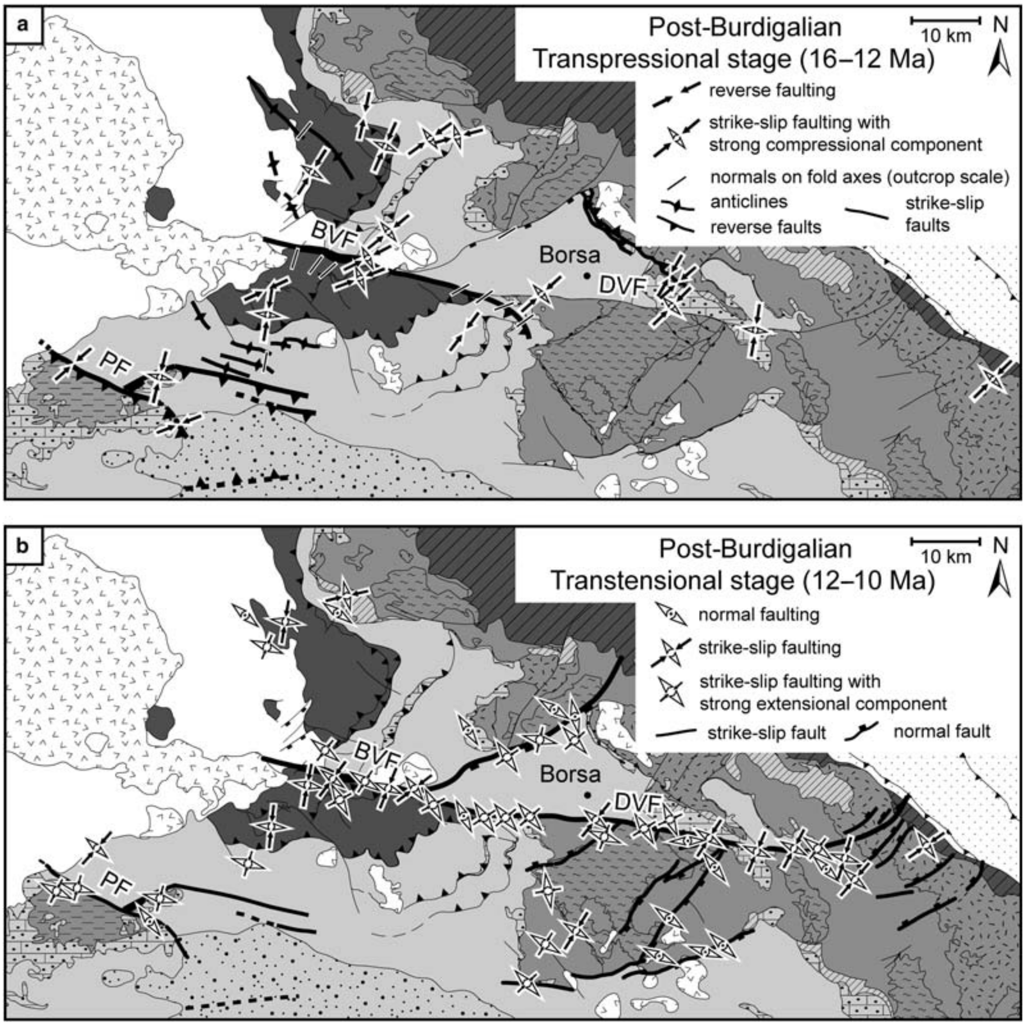

Fig. 3. Kinematics and structures related to the post-Burdigalian (16 to 10 Ma) tectonics in the study area (Tischler *et al.* 2006). The active structures are marked by thick lines (BVF = Bogdan–Voda fault, DVF = Dragos–Voda fault, PF = Preluca fault). A transpressional stage (**a**) precedes a transtensional stage (**b**), featuring constant SW–NE shortening. While the sinistral Bogdan–Voda fault is independently active during the transpressional stage (a), the Bogdan–Voda fault and Dragos–Voda fault are linked together during the transtensional stage (b).

S5 are from sedimentary units of the Pienides while S1 and S3 are from the post-tectonic Palaeogene to Early Miocene autochthonous cover of Tisza–Dacia (Late Oligocene Borsa sandstone). Samples have been taken from fine-grained sandstone horizons.

Zircon FT data

The zircon FT data are reported in Table 1. Zircon fission tracks were largely reset during the Cretaceous metamorphic overprint, associated with nappe stacking of the basement units.

The zircon fission track central ages of the Preluca massif and the Rodna horst range between 68.1 and 100.1 Ma (Fig. 4). Most samples pass the Chi-square test (Table 1, $\chi^2 > 5\%$). The zircon single grain age distributions show clusters (Fig. 4c, d) that indicate Late Cretaceous cooling (mainly Coniacian to Campanian) after a thermal event that led to full annealing of zircon (Fig. 4c, d), i.e. an event associated with temperatures exceeding 300 °C.

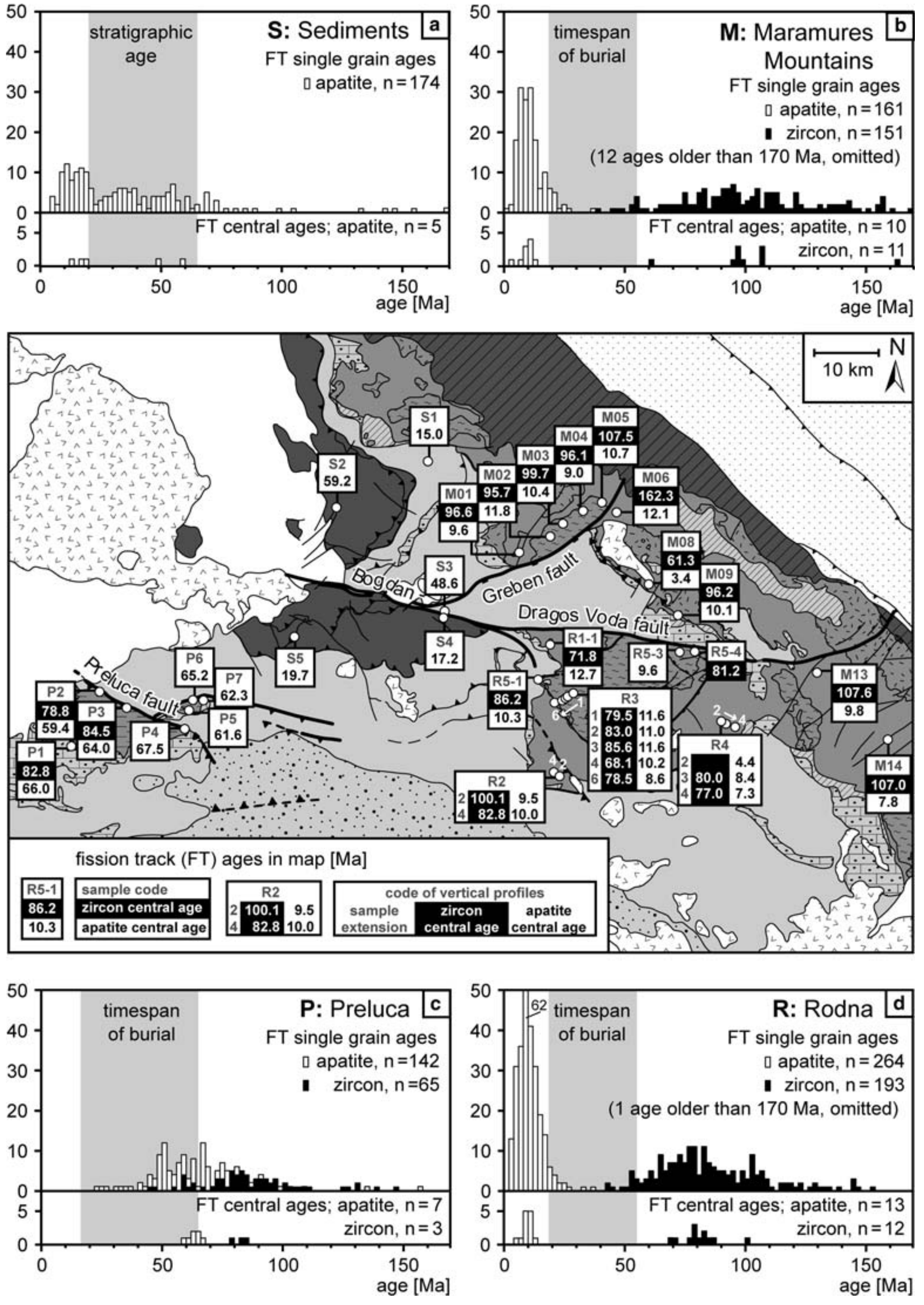

Fig. 4. Map indicating location of samples and results of the fission track analyses in terms of central ages, together with diagrams that summarize the single grain ages (a, b, c, d). In the sedimentary samples (**a**), the post-depositional thermal overprint caused strong annealing (S1, S4, S5), but also provenance single grain ages are preserved (S2, S3). In the Bucovinian nappe stack (**b**, **d**), apatite grains have been fully reset by the Palaeogene to Early Miocene burial, while zircon remained thermally undisturbed. Overlapping single grain ages of zircon and apatite from the Preluca massif reflect continuous exhumation through the ZPAZ and APAZ during the Late Cretaceous (**c**).

Table 1. *Zircon fission track data. All samples have been analysed using the external detector method (Gleadow 1981) with a zeta value (Hurford & Green 1983) of 141.40 ± 6.33 (Fish Canyon Tuff standard, CN1). Code: sample code; Latitude: latitude in WGS84; Longitude: longitude in WGS84; Alt. [m]: altitude above sea level; N Grains: number of grains counted; Ps [$\times 10^5$ cm^{-2}]: spontaneous track density; Ns: number of spontaneous tracks counted; Pi [$\times 10^5$ cm^{-2}]: induced track density; Ni: number of induced tracks counted; Pd [$\times 10^5$ cm^{-2}]: standard track density; Nd: number of standard tracks counted; χ^2 [%]: Chi-square probability (Galbraith 1981); Central age ±1σ [Ma]: zircon fission track central age (Galbraith & Laslett 1993)*

Code	Latitude	Longitude	Alt. [m]	N Grains	Ps [$\times 10^5$ cm^{-2}]	Ns	Pi [$\times 10^5$ cm^{-2}]	Ni	Pd [$\times 10^5$ cm^{-2}]	Nd	χ^2 [%]	Central Age ±1σ [Ma]
M01	24.496670	47.729790	540	10	176.37	1291	49.32	361	3.85	3065	34	96.6 ± 7.6
M02	24.560710	47.753720	580	4	109.39	367	30.10	101	3.77	3065	13	95.7 ± 13.5
M03	24.586640	47.772540	630	20	86.88	1468	35.45	599	5.80	3605	81	99.7 ± 6.8
M04	24.628100	47.791450	680	10	70.07	436	30.54	190	5.97	3605	84	96.1 ± 9.5
M05	24.667090	47.804300	745	20	98.44	2366	37.20	894	5.86	3605	<5	107.5 ± 7.4
M06	24.698590	47.790850	790	20	129.07	2543	33.35	657	5.91	3605	<5	162.3 ± 13.0
M08	24.770543	47.690263	820	20	123.09	2703	52.32	1149	3.69	3065	<5	61.3 ± 4.7
M09	24.833619	47.647505	1660	20	126.15	2501	32.18	638	3.50	3065	22	96.2 ± 6.5
M13	25.128220	47.571246	930	14	253.89	1812	58.71	419	3.54	3065	23	107.6 ± 8.5
M14	25.279510	47.478662	850	20	137.67	2830	30.60	629	3.38	3065	<5	107.0 ± 9.1
P1	23.574760	47.430957	315	14	79.60	1010	25.22	320	3.73	3065	55	82.8 ± 6.6
P2	23.628772	47.509842	215	16	155.74	1919	47.40	584	3.42	3065	38	78.8 ± 5.6
P3	23.686807	47.488712	610	35	128.38	3336	40.87	1062	3.81	3065	<5	84.5 ± 5.5
R1-1	24.559360	47.597860	1550	17	91.73	996	31.13	338	3.46	2967	25	71.8 ± 6.1
R2-2	24.597260	47.414920	1105	20	80.41	981	32.38	395	5.74	3605	78	100.1 ± 7.6
R2-4	24.590430	47.419300	705	26	115.20	2312	34.43	691	3.52	2967	12	82.8 ± 5.9
R3-1	24.620652	47.533782	2020	20	188.30	2550	55.68	754	3.35	3065	47	79.5 ± 5.1
R3-2	24.582850	47.423290	1465	20	74.15	1642	39.02	864	6.25	3605	62	83.0 ± 5.5
R3-3	24.608990	47.528930	1310	13	76.26	842	38.77	428	6.20	3605	37	85.6 ± 6.8
R3-4	24.604450	47.526330	1155	7	94.77	607	60.11	385	6.14	3605	50	68.1 ± 5.5
R3-6	24.587980	47.518690	945	20	92.24	934	49.77	504	6.03	3605	11	78.5 ± 6.4
R4-3	24.941010	47.494710	980	2	116.94	107	37.16	34	3.62	3065	86	80.0 ± 16.2
R4-4	24.960230	47.490430	700	20	134.72	1923	45.89	655	3.69	3065	<5	77.0 ± 5.8
R5-1	24.546451	47.552021	1150	8	204.11	635	57.54	179	3.46	3065	47	86.2 ± 8.4
R5-4	24.872870	47.596160	1270	20	161.18	2517	50.33	786	3.58	3065	10	81.2 ± 5.5

Some basement samples from the Maramures Mountains, however, yielded Cenomanian central ages (95.7 to 99.7 Ma; M01, M02, M03, M04, M09; Fig. 4b) which also pass the Chi-square test (Table 1, $\chi^2 > 5\%$). Hence they indicate earlier (Cenomanian) cooling after full annealing of zircon. In the most external samples (M05, M06, M13, M14), the coexistence of Late Cretaceous and Palaeozoic single grain ages (oldest single grain 310 Ma, M06; Appendix 1) indicates that annealing was only partial and was followed by Late Cenomanian cooling (Fig. 4b). Sample M08 with a younger Tertiary (61.3 Ma) central age forms an exception amongst this group.

No zircon FT single grain ages younger than Eocene have been found in samples from the basement units. Hence, it can be excluded that substantial heating, reaching temperatures within the ZPAZ, did result from Palaeogene to Early Miocene burial.

Apatite FT data

The apatite FT data are reported in Table 2. For the Preluca massif, an overlap between zircon and apatite single grain ages is observed (Fig. 4c). This overlap indicates continued slow cooling from temperatures above 200 °C down to temperatures below the lower limit of the APAZ (60 °C). The apatite central ages in the Preluca massif range from 59.4 to 67.5 Ma (Fig. 4c). A close look at the single grain age distribution reveals weak evidence for the existence of two clusters (Fig. 4c). Possibly the earlier cluster is related to Late Cretaceous cooling before renewed sedimentation. The second cluster could indicate partial annealing during Palaeogene to Early Miocene burial. Although etch pit long axes in the Preluca samples spread by at least 1 μm in each sample, suggesting compositional diversity, no clear correlation between etch pit long axis and single grain ages can be deduced (Appendix 2).

Three sedimentary samples (S1, autochthonous cover; S4 and S5, Pienides) show single grain ages that are younger than the stratigraphic age (Fig. 4a, Appendix 1). This indicates considerable post-depositional annealing. On the other hand, samples S2 (Pienides) and S3 (autochthonous cover) show single grain ages older than the stratigraphic age (Appendix 1).

In case of the samples from the Maramures Mountains and the Rodna horst, however, Palaeogene to Early Miocene burial caused total annealing of all apatite fission tracks (Fig. 4b, d). Central ages range between 7.3 and 12.7 Ma and thus indicate Middle to Late Miocene cooling. Two samples even yielded younger (Pliocene) central ages (M08: 3.4 Ma; R4-2: 4 Ma), best interpreted as indicating thermal overprint during Neogene volcanic activity (Pécskay *et al.* 1995). This interpretation is supported by the unusually young zircon FT central age of sample M08 (Fig. 4).

Confined track length measurements (Table 2) were used for thermal modelling of the apatite data that will be discussed below. In case of the sedimentary samples, the pre-depositional thermal history cannot be assumed to be identical for all constituent grains, hence confined track lengths were measured in dated grains only. In case of the basement samples, a common thermal history of individual samples allows for length measurements also in the non-dated grains (up to a maximum of 100 lengths). Only a limited number of samples provided sufficient track length data because of the low track densities. All basement samples show unimodal track length distributions, with mean values between 12.6 and 13.5 μm (Table 2). Sedimentary samples only provided a few track length data, which makes a characterization of the length distribution difficult.

Apatite (U–Th)/He data

The apatite (U–Th)/He data are reported in Table 3. In the Preluca massif, these apatite (U–Th)/He ages scatter and do not replicate within 2σ error. While the replicate of sample P4-II had small zircon inclusions and was therefore excluded, samples P3 and P4 both yielded apatite (U–Th)/He ages that are younger than the apatite FT single grain ages. Replicate ages from the Rodna massif yielded 12.0–13.3 Ma, which are, within 2σ error, indistinguishable from the accompanying apatite FT ages. This suggests fast cooling for the last stages of exhumation of the Rodna horst.

Thermal modelling of the apatite FT data

Thermal modelling used the apatite single grain ages and the confined track lengths as input data (Fig. 5). Additionally, time–temperature (t–T) constraints, independent from the apatite FT data, are incorporated. The t–T paths are modelled using the software AFTSolve (version 1.3.0, Ketcham *et al.* 2000) with the annealing model of Laslett *et al.* (1987). Modelling was done inverse monotonic with 10 000 runs for each model, using a Monte Carlo modelling scheme. Initial track length was 16.3 μm with a length reduction in age standard of 0.890. All models were run twice in order to identify reproducible trends.

In the case of the basement samples, such independent t–T constraints are given by the zircon FT central ages obtained on the same sample (or samples close by) and the age of the

Table 2. *Apatite fission track data. All samples have been analysed using the external detector method (Gleadow 1981) with a zeta value (Hurford & Green 1983) of 355.96 ± 9.39 (Durango standard, CN5). Code: sample code; Latitude: latitude in WGS84; Longitude: longitude in WGS84; Alt. [m]: altitude above sea level; N Grains: number of grains counted; Ps [$\times 10^5 cm^{-2}$]: spontaneous track density; Ns: number of spontaneous tracks counted; Pi [$\times 10^5 cm^{-2}$]: induced track density; Ni: number of induced tracks counted; Pd [$\times 10^5 cm^{-2}$]: standard track density; Nd: number of standard tracks counted; χ^2 [%]: Chi-square probability (Galbraith 1981); Central age ± 1σ [Ma]: apatite fission track central age (Galbraith & Laslett 1993); N Length: number of confined track lengths measured; Mean Length ± 1σ [μm]*

Code	Latitude	Longitude	Alt. [m]	N Grains	Ps [$\times 10^5$ cm^{-2}]	Ns	Pi [$\times 10^5$ cm^{-2}]	Ni	Pd [$\times 10^5$ cm^{-2}]	Nd	χ^2 [%]	Central Age ±1σ [Ma]	N Length	Mean Length ±1σ [μm]
M01	24.496670	47.729790	540	25	0.49	73	112.21	16596	119.59	6511	10	9.6 ± 1.2	–	–
M02	24.560710	47.753720	580	20	0.94	114	138.73	16842	98.14	6511	32	11.8 ± 1.2	–	–
M03	24.586640	47.772540	630	15	1.12	64	148.09	8471	77.35	3606	55	10.4 ± 1.3	–	–
M04	24.628100	47.791450	680	20	1.29	129	35.66	3580	14.10	4605	58	9.0 ± 0.9	80	12.94 ± 2.21
M05	24.667090	47.804300	745	20	2.24	168	28.73	2155	7.74	4223	99	10.7 ± 0.9	100	12.98 ± 3.20
M06	24.698590	47.790850	790	3	0.51	10	87.59	1708	116.61	4196	39	12.1 ± 3.9	–	–
M08	24.770543	47.690263	820	2	0.98	4	43.90	180	8.52	4451	60	3.4 ± 1.7	–	–
M09	24.833619	47.647505	1660	16	0.53	31	90.19	5276	96.19	5773	99	10.1 ± 1.8	–	–
M13	25.128220	47.571246	930	20	0.44	64	8.57	1261	10.81	4451	99	9.8 ± 1.3	–	–
M14	25.279510	47.478662	850	20	1.34	152	32.43	3668	10.50	4451	26	7.8 ± 0.7	43	13.35 ± 2.12
P1	23.574760	47.430957	315	20	3.06	297	8.40	815	10.23	4223	65	66.0 ± 4.9	100	13.01 ± 2.54
P2	23.628772	47.509842	215	20	6.33	713	16.79	1892	8.93	4223	9	59.4 ± 3.7	100	12.98 ± 1.92
P3	23.686807	47.488712	610	20	6.93	671	18.18	1760	9.37	4223	<5	64.0 ± 4.6	100	12.86 ± 1.70
P4	23.810507	47.465312	350	22	1.09	150	26.93	3724	94.57	6511	43	67.5 ± 6.0	–	–
P5	23.817260	47.488947	390	20	18.13	2489	44.93	6169	8.50	4223	<5	61.6 ± 3.0	100	12.75 ± 1.23
P6	23.824540	47.503686	430	20	14.12	1028	37.89	2758	9.80	4223	<5	65.2 ± 4.0	100	12.62 ± 2.08
P7	23.846548	47.503894	380	20	4.84	456	15.72	1482	11.44	4451	94	62.3 ± 3.8	100	12.60 ± 1.90
R1-1	24.559360	47.597860	1550	20	0.58	41	11.86	837	14.55	4766	97	12.7 ± 2.1	–	–
R2-2	24.597260	47.414920	1105	20	0.41	63	93.25	14333	121.63	4196	92	9.5 ± 1.2	–	–
R2-4	24.590430	47.419300	705	20	0.52	51	108.36	10717	118.28	4196	88	10.0 ± 1.4	100	12.80 ± 2.65
R3-1	24.620652	47.533782	2020	24	4.41	539	65.71	8030	9.78	4451	8	11.6 ± 0.7	59	13.12 ± 2.79
R3-2	24.582850	47.423290	1465	20	2.55	357	54.69	7646	13.04	4766	10	11.0 ± 0.8	100	13.50 ± 2.20
R3-3	24.608990	47.528930	1310	20	2.48	496	48.58	9716	12.79	4766	13	11.6 ± 0.7	100	13.25 ± 2.31
R3-4	24.604450	47.526330	1155	20	0.38	50	8.30	1096	12.54	4766	99	10.2 ± 1.5	–	–
R3-6	24.587980	47.518690	945	20	0.94	111	15.89	1873	8.17	4223	79	8.6 ± 0.9	–	–
R4-2	24.931050	47.498160	1305	20	0.72	85	38.19	4499	13.00	4451	46	4.4 ± 0.5	–	–
R4-3	24.941010	47.494710	980	20	2.02	216	53.45	5730	12.48	4451	84	8.4 ± 0.6	64	12.81 ± 2.48
R4-4	24.960230	47.490430	700	20	0.89	73	26.52	2185	12.27	4451	95	7.3 ± 0.9	–	–
R5-1	24.546451	47.552021	1150	20	1.31	93	20.94	1487	9.26	4451	93	10.3 ± 1.1	–	–
R5-3	24.951870	47.550260	1400	20	3.02	218	51.72	3734	9.22	4557	8	9.6 ± 0.9	100	13.32 ± 2.45
S1	24.296360	47.854000	550	38	2.69	514	41.23	7884	12.91	4605	29	15.0 ± 0.9	15	13.68 ± 2.01
S2	24.111950	47.782210	350	39	9.25	1787	33.57	6489	10.97	4605	<5	59.2 ± 5.0	61	12.14 ± 2.09
S3	24.351650	47.641020	530	40	7.21	1500	32.93	6850	12.27	4605	<5	48.6 ± 3.0	35	12.47 ± 2.33
S4	24.348370	47.635130	555	21	1.61	174	21.52	2320	12.59	4605	12	17.2 ± 1.6	–	–
S5	24.030170	47.599060	555	36	1.48	242	129.53	21178	94.83	4196	<5	19.7 ± 2.2	19	10.08 ± 2.71

Table 3. *Apatite (U–Th)/He data. Analyses of one Durango apatite standard aliquot (two grains) yield 33.1 ± 0.7 Ma. Code: sample code; ^{4}He [cc STP]: concentration of ^{4}He; U^{238} [ng]: concentration of U^{238}; Th^{232} [ng]: concentration of Th^{232}; Th/U: Th^{232}/U^{238} ratio; (U–Th)/He Age [Ma]; Ft: correction of α-recoil (Farley 2002); Corrected (U–Th)/He Age [Ma]; Error 2σ; FT Central age ±1σ[Ma]: apatite fission track central age (Galbraith & Laslett 1993)*

Code	4He [cc STP]	U^{238} [ng]	Th^{232} [ng]	Th/U	(U–Th)/He Age [Ma]	Ft	Corrected (U–Th)/He Age [Ma]	Error 2σ	FT Central Age ±1σ [Ma]
P3-I	4.29E-11	0.015	0.009	0.6	20.5	0.68	30.1	3.0	64.0 ± 4.6
P3-II	4.75E-11	0.025	0.018	0.7	13.4	0.69	19.3	1.9	
P4-I	5.79E-11	0.054	0.027	0.5	7.9	0.82	9.6	1.0	67.5 ± 6.0
P4-II	9.21E-11	0.014	0.045	3.2	30.6	0.80	38.3	3.8	
R2-4-I	1.54E-10	0.114	0.030	0.3	10.4	0.78	13.3	1.3	10.0 ± 1.4
R2-4-II	7.55E-11	0.058	0.027	0.5	9.6	0.80	12.0	1.2	
R3-2-1	8.00E-10	0.657	0.033	0.0	9.8	0.76	12.9	1.3	11.0 ± 0.8

unconformably overlying sediments. In the case of the Preluca massif, the time of maximum burial can also be constrained by assuming it to coincide with the end of Burdigalian sedimentation (Hida beds: 16 Ma). In the Bucovinian nappe stack, maximum burial temperatures are assumed to have been reached by a combination of sedimentary and tectonic burial during imbrication of the autochthonous sediments related to thrusting of the Pienides (18.5 Ma, Tischler *et al.* 2006).

Regarding the sedimentary samples, one t–T constraint is given by the stratigraphic age of the dated sediment (Săndulescu & Russo-Săndulescu 1981; Săndulescu *et al.* 1991; Aroldi 2001). Interestingly, a pre-Tertiary heating event has to be assumed in order to allow for the modelling of samples S2 and S3. The timing of maximum burial of the samples from the Pienide nappes (S2 and S5) is inferred to immediately pre-date nappe emplacement (20 Ma, Tischler *et al.* 2006), since erosion of the Pienides during thrusting is indicated by the deposition of a Burdigalian clastic wedge. In the case of the autochthonous cover (samples S1 and S3), the overthrusting of the Pienides is considered to have caused additional burial. Hence it was assumed that maximum temperatures were reached at the end of nappe emplacement (18.5 Ma, Tischler *et al.* 2006).

In the case of the Preluca massif, Palaeogene to Early Miocene burial caused partial annealing of apatite (Fig. 6). Late Cretaceous to Early Tertiary cooling is constrained by the zircon FT data and by the sedimentary unconformity. Thermal modelling suggests an increase of maximum temperatures from around 60 °C (P1) in the SW to around 80 °C in the NE (P5, P7), interpreted in terms of an increasing amount of burial towards the NE. The modelled maximum temperature near the Preluca fault (sample P3, 69 °C) in the upper part of the apatite helium partial retention zone is in good

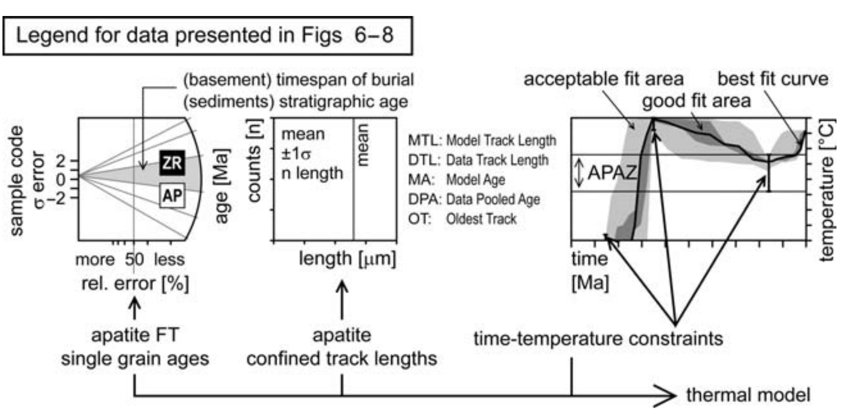

Fig. 5. Diagram explaining the thermal modelling of apatite FT data. This figure also serves as a legend for Figures 6–8. The single grain ages and the confined track lengths provide input data. Using additional independent constraints (e.g. zircon FT data, stratigraphic information), t–T paths fitting the data are modelled.

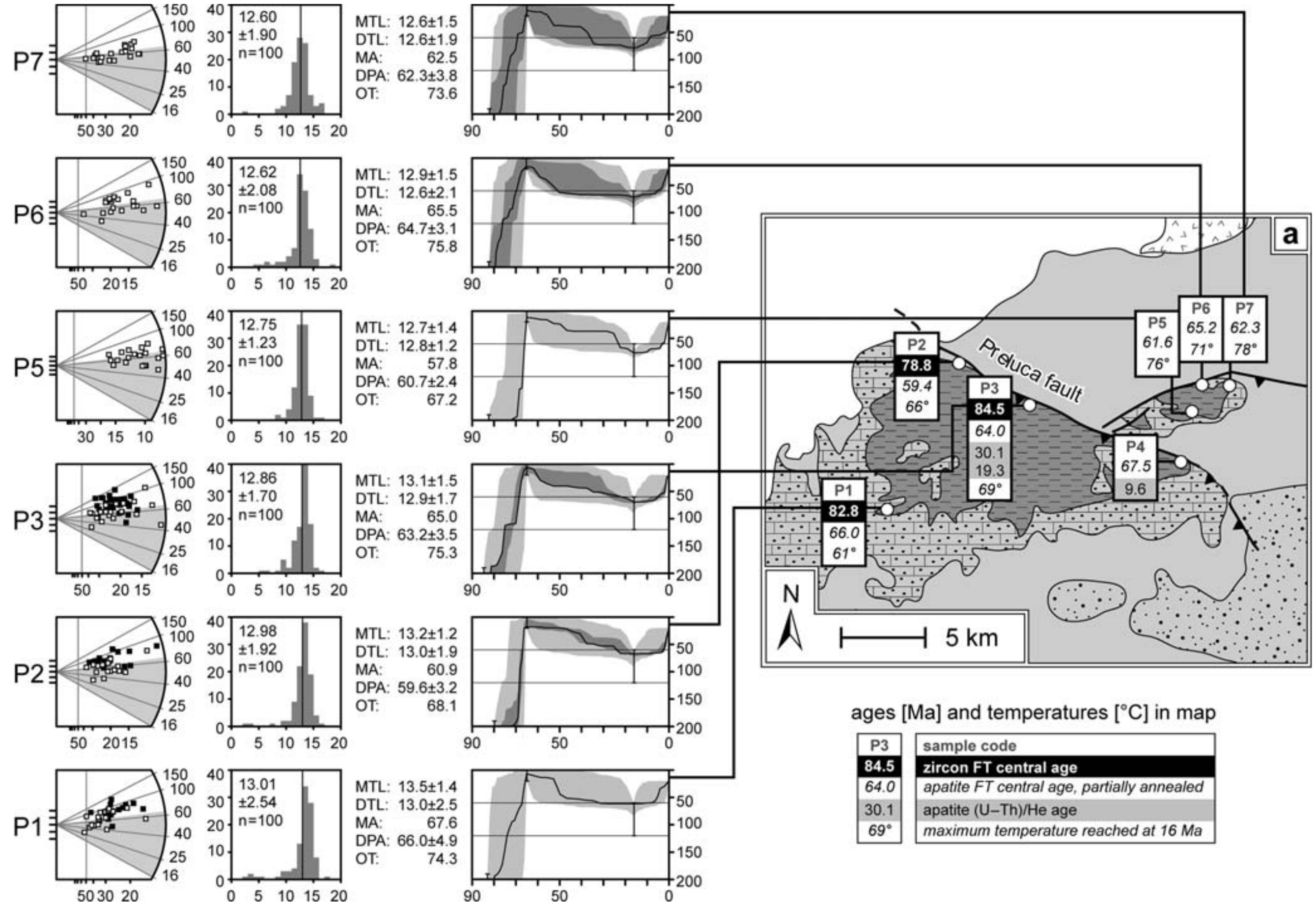

Fig. 6. Thermal modelling of apatite FT data in the Preluca massif. All radial plots (Galbraith 1990) show the same age spectrum to allow for direct comparison. Burial heating by the deposition of Palaeogene to Early Miocene sediments caused partial annealing of fission tracks in apatite. The models slightly indicate a deepening in burial by sedimentation from SW to NE, reflected by the increasing maximum temperatures modelled (**a**). The temperatures reached at the Preluca fault (69 °C) are confirmed by partial (P3) and full retention (P4) of He in apatite.

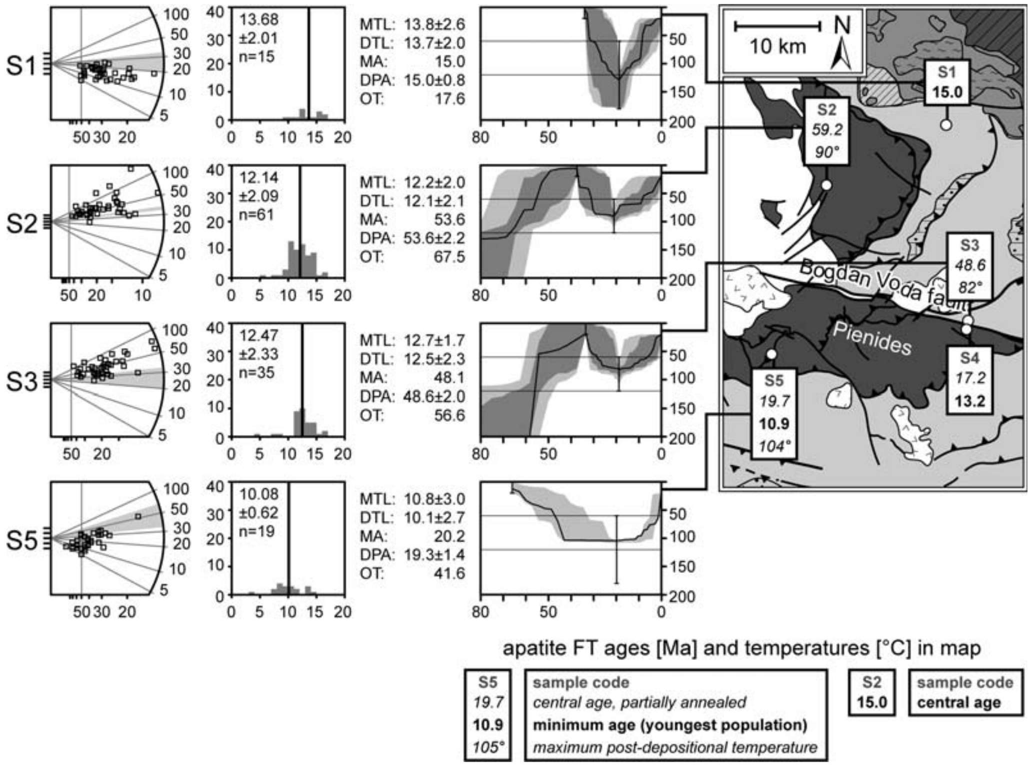

Fig. 7. Thermal modelling of apatite FT data from the sedimentary units. All radial plots (Galbraith 1990) show the same age spectrum to allow for direct comparison. All samples show at least post-depositional partial annealing of fission tracks in apatite; S1 has been fully annealed after deposition. Due to strong annealing in S4 and S5, minimum ages of the youngest populations were calculated. These minimum ages and the central age of S1 indicate Middle to Late Miocene cooling.

agreement with full (P4) and partial (P3) retention of helium, as is indicated by the (U–Th)/He data.

For samples S2 and S3, thermal modelling indicates heating to temperatures within the APAZ, followed by slow cooling (Fig. 7). The thermal history of S1, on the other hand, is characterized by fast heating to temperatures above the APAZ directly preceding fast cooling to temperatures within the APAZ. This short-lived thermal pulse is most likely related to the overthrusting by the Pienides. The thermal modelling of sample S5 shows that cooling from maximum temperatures occurred after 10 Ma (Fig. 7). The youngest grain populations in the strongly annealed samples south of the Bogdan–Voda fault indicate cooling during the Middle (S4: 13.2 Ma) and Late Miocene (S5: 10.9 Ma).

In the case of the Bucovinian nappe stack, the exhumation and burial history before 18.5 Ma was also modelled for all samples. However, due to the complete annealing of pre-Miocene apatite fission tracks, the track parameters are only sensitive regarding the final stages of exhumation (Fig. 8). The complete cooling paths, including the pre-Tertiary history, are only depicted for sample M14 (exemplary for the Maramures Mountains, Fig. 8a) and for R5-3 (exemplary for the Rodna horst, Fig. 8b). Both the zircon FT data and a sedimentary unconformity constrain Late Cretaceous to Eocene cooling in the Rodna horst. In the Maramures Mountains, however, the basement has already been exhumed in Cenomanian times. After maximum burial and heating at 18.5 Ma, most samples enter the upper limit of the APAZ between 15 and 12 Ma before present, and enhanced cooling occurred generally between 10 and 7 Ma.

Revealing the Miocene exhumation history of the Rodna horst

By integrating information provided by the available geological maps (Kräutner *et al.* 1978, 1982, 1983,

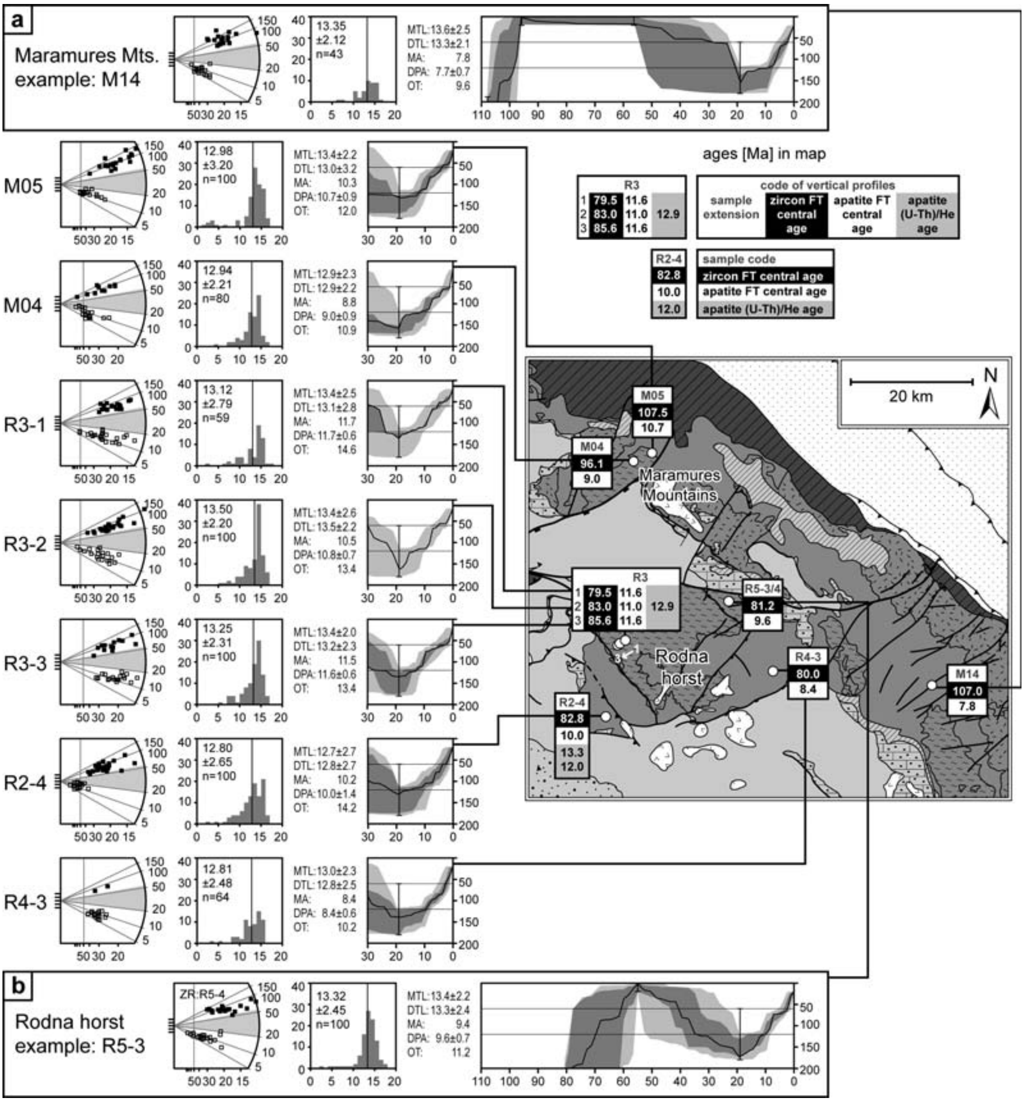

Fig. 8. Thermal modelling of samples from the Bucovinian nappe stack. All radial plots (Galbraith 1990) show the same age spectrum to allow for direct comparison. Because apatite has been fully annealed during Palaeogene to Early Miocene burial, the modelled t–T paths are tightly constrained only for the last stages of Miocene exhumation. Therefore, the results of the complete modelling, starting in the Cretaceous, are only given for the samples M14 (**a**) and R5-3 (**b**), which serve as examples for the Maramures Mountains and the Rodna horst, respectively.

1989) and by constructing schematic cross-sections (Fig. 9c, d), the progressive exhumation of a more internal part of the Bucovinian nappe stack—the Rodna horst—will now be discussed in four time slices (Fig. 10). The schematic cross-section 1 (Fig. 9c) depicts reverse faulting and open folding (5% profile-parallel shortening) related to the post-Burdigalian transpressional stage. In the perpendicular cross-section 2, however, normal faulting related to the subsequent transtensional stage is more evident (Fig. 9d, 7% profile-parallel extension). In section 1, the base Oligocene is tilted to the SW by some 3°, locally reaching up to 5° in the central block of the Rodna horst (Fig. 9b). Lines indicating 5° and 3° tilt are given for comparison in Fig. 9b. Two SW–NE striking normal faults

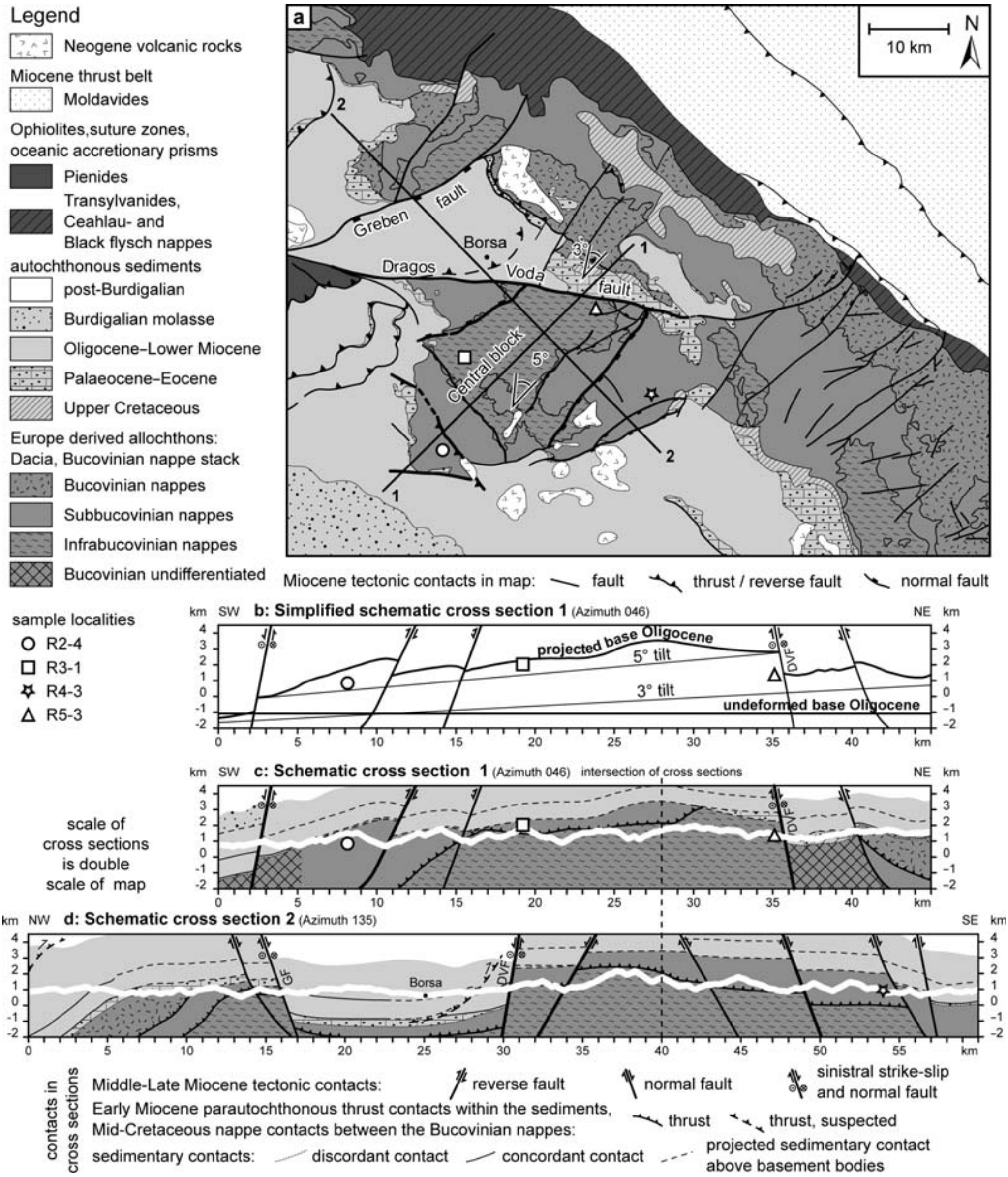

Fig. 9. Map (**a**) and schematic cross-sections (**b, c, d**) through the Bucovinian nappe stack in the study area. Schematic cross-section 1 (c) documents reverse faulting and open folding during the Middle Miocene transpressional stage, while section 2 (d) documents extension by normal faulting during the Middle to Late Miocene transtensional stage. The base of the Oligocene shows a general tilt towards the SW by approximately 3° (b). Along the central block of the Rodna horst, the tilt to the SW increases to 5°, realised along two normal faults delimiting this block by an increasing offset towards the Dragos–Voda fault (a). The suspected thrust at Borsa is drawn after Săndulescu pers. comm. 2002 ('Duplicature de Borsa').

(Fig. 9a), delimiting the central block, allow for this additional tilting. Offset across these normal faults increases towards the Dragos–Voda fault. This indicates that tilting occurred predominantly during the transtensional stage since deformation related to the transtensional stage dominates along the Dragos–Voda fault segment, delimiting the Rodna horst towards the north.

In the following, vertical movements predicted by structural observations are integrated with results from apatite FT thermal modelling in order to reconstruct the exhumation history of the Rodna horst. Relative uplift visible in cross-sections 1 and 2 (Fig. 9c, d) is estimated and correlated with Middle to Late Miocene brittle tectonics which occurred between 16 and 10 Ma ago (Tischler *et al.* 2006). Timing and amount of these vertical movements (Fig. 10, column B) are then directly compared to the modelled best-fit t–T paths inferred from apatite FT data obtained from the Rodna horst (Fig. 10, column C).

The undeformed base of the Oligocene deposits is used as a reference for differential tectonic uplift (Fig. 9b; Fig. 10, column B) and is defined as the null datum for the starting point at 20 Ma ago (Fig. 10Ba). All the subsequent time slices (Fig. 10Bb to Bd) show this reference plane ('undeformed base Oligocene') for comparison.

20 to 16 Ma time slice (Fig. 10, Row a)

This time slice shows the relative altitudes of the samples before the onset of Miocene brittle deformations 16 Ma ago (Tischler *et al.* 2006). The geological cross-sections (Fig. 9c, d) allow for an estimate of the original position of the samples relative to the base Oligocene (reference plane 'undeformed base Oligocene') at the following relative altitudes in Fig. 10Ba: R2-4 at −800 m, R3-1 at −200 m, R4-3 at −1000 m and R5-3 at −1400 m. The modelled t–T paths inferred from apatite FT data show that no significant cooling occurred before 16 Ma. All samples remain at temperatures above the APAZ (Fig. 10Ca).

16 to 12 Ma time slice: transpressional stage (Fig. 10, Row b)

During this transpressional stage, three tectonic features influencing tectonic uplift can be identified in cross-section 1 (Fig. 9c):

(1) Reverse faulting affects the SW corner of the Rodna horst. This reverse faulting influences only sample R2-4, situated in a hanging-wall position.

(2) Tilting is interpreted to play a subordinate role during the transpressional stage. Out of a total amount of 5°, only about 1° is assumed to have commenced between 16 and 12 Ma. The amount of relative uplift during tilting is estimated along cross-section 1, and is given by the vertical distance between a horizontal line and a line tilted 1° towards the SW, intersecting at the southern boundary fault of the Rodna horst (Fig. 9a). This vertical distance has been measured at the respective sample locations in section 1. The projected position of sample R4-3 is at the intersection of both sections.

(3) Additional relative tectonic uplift is realised by open folding in the cases of samples R3-2 and R4-3 in an anticlinal position, while R5-3 is situated in a synclinal position. The effect of open folding has been estimated by constructing the distance of the sample location to a tangent onto the synclines.

From the relative position of the specimens at the end of this stage (Fig. 10Bb), the following amounts of tectonically induced relative uplift can be deduced for this stage: +1300 m for R2-4, +1000 m for R3-1, +1000 m for R4-3 and +600 m for R5-3. Note that R2-4 and R3-1 are above the reference line at the end of this stage.

The uplift produced during the transpressional stage relative to the reference line base Oligocene causes a phase of slow cooling visible in the t–T paths (16 to 11 Ma interval in Fig. 10Cb). R3-1 and R2-4 enter the APAZ at very low cooling rates (cooling paths with a gradient of about 2.5 °C/Ma), while R4-3 and R5-3 remain at higher temperatures.

12 to 10 Ma time slice: transtensional stage (Fig. 10, Row c)

Normal and strike-slip faulting, together with 4° SW tilting led to variable amounts of relative tectonic uplift during this transtensional stage. First the amount of uplift produced by this tilting (4°) is estimated. Secondly, an additional uplift of the whole tilted block, as documented by an offset at its SW boundary fault, was applied. The amount of relative uplift for sample R4-3 is derived from its position projected into cross-section 1, corrected for normal faulting visible in cross-section 2. The tectonic uplift produced during this transtensional stage relative to the reference line (Fig. 10Bc) amounts to: +1400 m for R2-4, +2400 m for R3-1, +2200 m for R4-3 and +3400 m for R5-3. The relatively greater uplift values deduced for R3-1 and R5-3 result in their higher position relative to R2-4 and R4-3.

Relative tectonic uplift and erosion during the transtensional stage result in a phase of enhanced exhumation and cooling visible in the t–T paths (11 to 7 Ma interval of Fig. 10Cc). R5-3 enters and nearly crosses the APAZ at high cooling rates (the cooling path indicates 24 °C/Ma). At the end of this phase of enhanced cooling, R3-1 and R5-3 are at the lower limit of the APAZ, while R2-4 and R4-3 remain at higher temperatures. The relatively high cooling rates associated with this extensional stage resulted in Middle to Late Miocene apatite FT central ages in the Rodna horst.

10 to 0 Ma time slice (Fig. 10, Row d)

After cessation of the tectonic activity at 10 Ma (Tischler *et al.* 2006), the samples reached their present-day altitude relative to the 'undeformed base Oligocene' (Fig. 10Bd) at the following

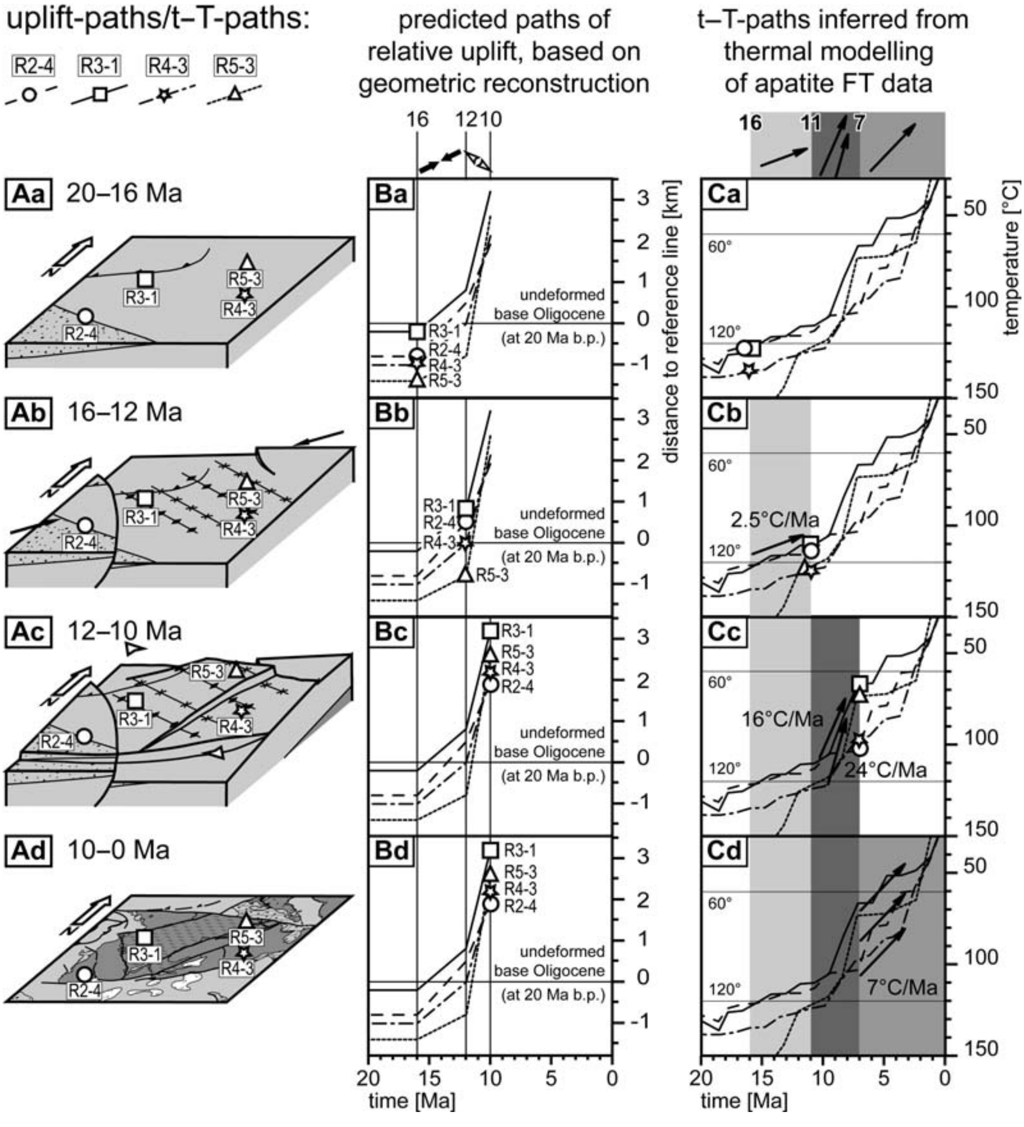

Fig. 10. Direct comparison of unscaled and schematic tectonic sketches (Column A), relative tectonic uplift paths (Column B) and cooling paths (best fit of 10 000 runs) inferred from thermal modelling of apatite FT data (Column C) in the Rodna horst, from top to bottom, four subsequent time intervals (see column A). Amounts of relative tectonic uplift are estimated in respect to the undeformed base Oligocene (Fig. 9b). Greyscale in column C denotes time intervals and associated changes in the rate of cooling (dark = fast cooling).

relative altitudes: +1900 m for R2-4, +2600 m for R5-3, +2200 m for R4-3 and +3200 m for R3-1. Final cooling to surface temperatures was associated with medium cooling rates of about 7 °C/Ma according to the cooling paths (Fig. 10Cd).

Summary of the Miocene exhumation history deduced for the Rodna horst

The Miocene cooling and exhumation observed in the Rodna horst is the result of a combination of tectonic uplift and erosion. Relative tectonic uplift during the transpressional stage (16 to12 Ma), together with exhumation by erosion, allowed for the observed slow cooling (16 to 11 Ma). The transtensional stage (12 to10 Ma), however, is reflected in a phase of enhanced cooling (11 to 7 Ma) related to a combination of tectonic and erosional exhumation. Although tectonic uplift and cooling are not contemporaneous, the tectonic stages are reflected in both relative uplift paths and cooling paths. During the transpressional stage (Fig. 10Ba

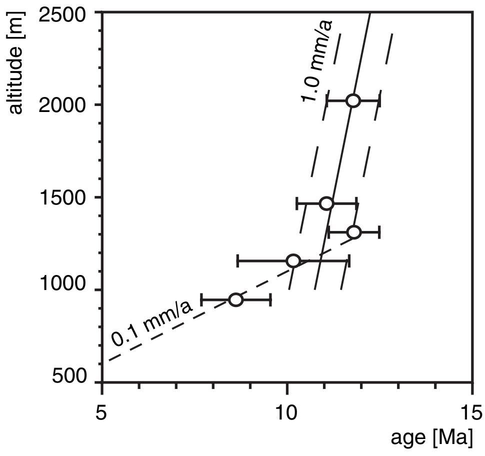

Fig. 11. Altitude vs. age plot of vertical profile R3 (Rodna horst), suggesting a two-stage exhumation history: enhanced exhumation of at least 1.0 mm/a between 12 and 11 Ma, followed by slower exhumation after 10 Ma. 1.0 mm/a and 0.1 mm/a lines are given as a reference.

to Bb) R3-1 and R2-4 are uplifted above the 'undeformed base Oligocene' during their cooling below the upper temperature limit of the APAZ (Fig. 10Ca to Cb). This implies that the reference plane 'undeformed base Oligocene' reflects a temperature interval close to the upper limit of the APAZ (i.e. 120 °C). Based on this observation, the base of the Oligocene sediments is estimated to have been subjected to temperatures around the upper limit of the APAZ by the beginning of Middle Miocene times. This estimation is corroborated by full annealing of apatite fission tracks, as is observed in Eocene sediments located east of Borsa (Sanders 1998).

An exhumation rate for the Rodna horst can be calculated via the altitude vs. age relation, extracted from the vertical profile R3 (Fig. 11). Enhanced exhumation rates are deduced for the time interval 12 to 11 Ma ($\geq$1.0 mm/a), followed by overall slow exhumation after 10 Ma before present (the 0.1 mm/a-line is given as reference). Thus the altitude vs. age relationship corroborates the stratigraphic dating as well as the predominance of the transtensional stage along the Dragos–Voda fault.

Revealing the total amount of Miocene exhumation for the entire study area

The total amount of Miocene exhumation in the study area depicted in Fig. 12 has been estimated on the base of the apatite FT data. The maximum palaeodepth (D_{max}) is estimated on the basis of the maximum palaeotemperature (T_{max}), assuming a geothermal gradient of $\Delta T/\Delta Z = 20\ ^{\circ}C/km$ and an estimated surface temperature of 10 °C (T_s) on the basis of:

$$D_{max} = (T_{max} - T_s)/(\Delta T/\Delta Z)$$

A geothermal gradient of 20 °C/km has been derived by Sanders (1998), who balanced erosion along the Carpathian and Apuseni Mountains against the sedimentary infill of the Transylvanian basin. 20 °C/km is also in accordance with present-day heat-flow data (Veliciu & Visarion 1984; Demetrescu & Veliciu 1991). However, a palaeogeothermal gradient is not easy to quantify. The area is affected by volcanism, which may provide additional heat sources. Therefore, the given amounts of exhumation represent maximum values.

In the case of samples displaying only partial annealing of apatite (samples P1, P2, P3, P5, P6, P7, S2, S3 and S5), thermal modelling indicates that T_{max} was reached before the onset of Miocene exhumation. In the case of fully annealed apatite (profiles R1, R2, R3, R4, R5, samples M01, M02, M03, M04, M05, M06, M08, M09, M13, M14 and S1), T_{max} has to have exceeded 120 °C. Thermally undisturbed zircon in all basement samples excludes temperatures above the lower limit of the ZPAZ ($T_{max} < 190\ ^{\circ}C$) during Palaeogene to Early Miocene burial.

In the case of some samples (profiles R1, R2, R3, R4, R5, samples M01, M09), the estimation of T_{max} has been improved by assuming that the base of the Oligocene approximates the upper limit of the APAZ (120 °C, see above) before the onset of exhumation. In these cases, T_{max} can be derived by the vertical distance of the sample location to the base Oligocene based on maps and cross-sections (Fig. 9) and the estimated geothermal gradient of 20 °C/km. T_{max} for S4 has been estimated to 100 °C, in analogy to S5 since both samples show strong, but not full, annealing. All palaeodepth, and hence also all exhumation values, given in Figure 12 are rounded to 0.5 km intervals.

The Middle to Late Miocene cooling ages (central ages, youngest populations: 15.0 to 7.3 Ma) indicate that the entire amount of cooling and exhumation is the result of erosion that followed tectonic uplift during the strike-slip dominated post-Burdigalian tectonic activity in the study area. However, in the area directly north of the Bogdan–Voda fault, the total amount of exhumation (S2: 4.0 km, S3: 3.5 km) can hardly be exclusively of post-Burdigalian age, since the altitude of the base of the Middle Miocene sediments is found close to that of the collected samples. Hence, north of the Bogdan–Voda fault a significant part of the total amount of exhumation

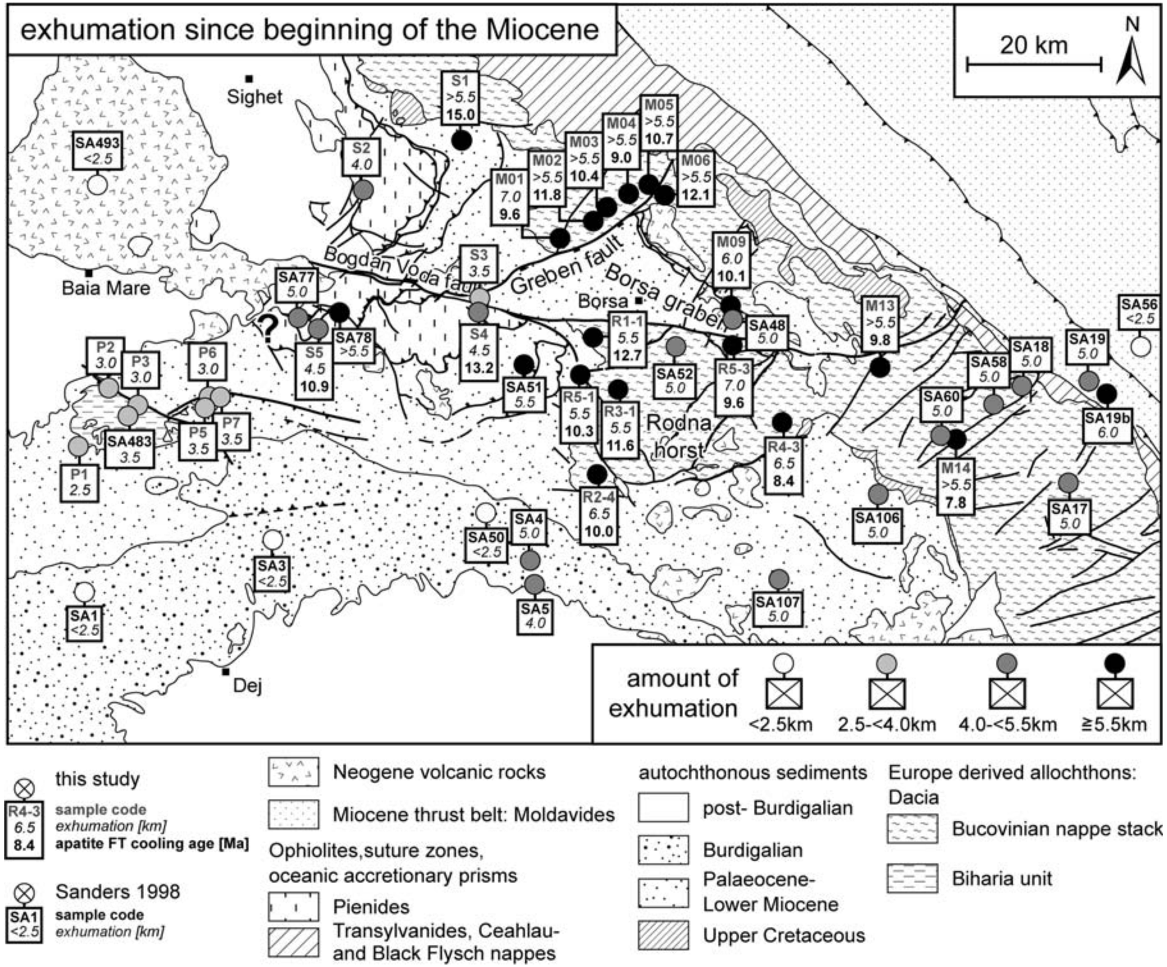

Fig. 12. Map showing the calculated amounts of Miocene exhumation in the study area. The amount of exhumation is given by the maximum palaeotemperatures inferred from apatite FT data, assuming a geothermal gradient of 20 °C/km. Sample code SA refers to additional data from Sanders (1998). For most samples, the entire amount of exhumation was realised after Middle Miocene times (i.e. after 16 Ma), as is indicated by Middle to Late Miocene cooling ages.

seems to be due to erosion that occurred earlier, i.e. during and directly following the intra-Burdigalian thrusting of the Pienides.

The strong thermal pulse found in the westernmost area of the southern part of the Pienide nappes (marked by a question mark, Fig. 12) occurred relatively late, as is indicated by young cooling ages: 10.9 Ma for the youngest population (Fig. 12), 11 Ma and 8 Ma according to Sanders (1998). Since the base of Middle Miocene sediments is in close neighbourhood, a thermal pulse caused by burial is rather unlikely. Hence, we interpret these Late Miocene cooling ages to be the result of a hydrothermal overprint. An intensive overprint of the sedimentary units of the Pienides close to the volcanic body at Baia Mare is documented by Săndulescu & Russo-Săndulescu (1981). Whether partial annealing is related to hydrothermal overprint or to heating by burial is difficult to judge.

Recapitulation of results

Burial by Palaeogene to Early Miocene sediments, locally combined with thrusting and frontal imbrication, caused full annealing of fission tracks in apatite in the case of the samples from the Bucovinian nappe stack. Locally, this is also the case for the sedimentary cover. Regarding the Preluca massif located in the SW part of the study area, however, the amount of burial due to the sedimentary overburden as well as the amount of exhumation were less substantial. Fission tracks in apatite from the Preluca massif remained relatively undisturbed during heating by burial, while (U–Th)/He data document considerable retention of He.

Exhumation is mainly the result of erosion triggered by uplift, accompanying and/or following post-Burdigalian strike-slip tectonic activity along the Bogdan–Dragos–Voda fault system. Middle Miocene cooling ages (15.0 to 13.2 Ma) document exhumation during a first transpressional stage in the eastern part of the study area (Fig. 12). In the central part of the study area, Middle to Late Miocene ages (12.7 to 7.3 Ma) indicate enhanced cooling and exhumation during and following a second transtensional stage. The vertical profile R3 indicates enhanced exhumation of at least 1 mm/a between 12 to 11 Ma (Fig. 11). Enhanced final exhumation is confirmed by apatite (U–Th)/He ages which coincide with the accompanying apatite FT ages within the error limits.

Discussion

Hydrothermal overprint

Beyond the Miocene cooling ages, a few Pliocene apatite FT central ages were also obtained in samples from the Bucovinian nappes (3.4 Ma for M08, 4.4 Ma for R4-2). Neogene volcanic activity is a likely explanation for these young ages. However, volcanism started in the Middle Miocene and activity only lasted until 9.0 Ma north of Baia Mare and 8.6 Ma in the area of the Rodna horst, respectively (Pécskay *et al.* 1995). Even though a second, younger phase of volcanism can be observed north of Baia Mare (8.1 to 6.9 Ma, Pécskay *et al.* 1995), Pliocene volcanism is only documented for areas located some 80 to 100 km south of our study area (Harghita Mountains). Thus we propose that the observed late annealing of apatite is due to hydrothermal activity that postdates active volcanism. The present-day occurrence of hot springs at the southern margin of the Rodna horst also favours such an interpretation.

Burial and exhumation in the study area

The overall decrease in the amount of burial towards the SW, as deduced from the thermochronological data, is in accordance with the diminishing thickness of Oligocene sediments towards the SW (de Brouker *et al.* 1998). At the southern rim of the Preluca massif, apatite FT data indicate 2.5 km of burial (assuming a geothermal gradient of 20 °C; Fig. 12). About 0.8 km of Palaeocene to Early Miocene (Aquitanian) sediments are still preserved in this area (Rusu *et al.* 1983). Values of 2500 km for the total sedimentary overburden are in good accordance with the thickness of the Burdigalian strata which reaches about 2 km in the Transylvanian basin directly to the south, as is documented in seismic sections (de Broucker *et al.* 1998; Ciulavu *et al.* 2002; Tischler *et al.* 2008).

Concerning the area of the Rodna horst, our apatite FT data suggest that 5.5 km of sediments accumulated above the base Oligocene. A minimum thickness of Oligocene deposits of 2.8 km is documented in the area of Borsa (Kräutner *et al.* 1982). Geometric projections of the Oligocene deposits in the profiles of Figure 9c and 9d, based on available maps (Ianovici *et al.* 1968; Kräutner *et al.* 1989; Săndulescu *et al.* 1991), indicate a minimum thickness which diminishes from 4.4 km NW of the Greben fault to 2.7 km SW of the Rodna horst. Higher burial depths in the NW part of the study area are directly documented by the fully annealed apatite FT sample S1 from the Oligocene deposits of this area. Yet the observed or inferred thickness of the post-Eocene deposits is still insufficient for explaining the burial depth inferred from our FT data. Excess burial can be explained by additional tectonic loading related to the emplacement of the Pienides during the Burdigalian and accompanying imbrications of the autochthonous cover (Tischler *et al.* 2006). Especially in the NW parts of the

Rodna horst, additional tectonic burial appears to be indicated by tectonic considerations. In the SE corner of the Rodna horst, however, additional Burdigalian deposits could also allow for the necessary total overburden. However, it has to be kept in mind that a higher geothermal gradient than the assumed 20 °C/km can also explain apparent discrepancies between palaeotemperatures and amounts of overburden. The apparent volcanic activity in the area may have increased the geothermal gradient. Therefore, the mentioned values for post-Miocene exhumation (Fig. 12) should be considered as maximum estimates.

Although the emplacement of the Pienide nappes probably led to tectonic burial in most parts of the study area, certainly in parts of the autochthonous sediments adjacent to the frontal thrust (sample S1), exhumation that accompanied or postdated the emplacement of the Pienides is indicated by the truncation of tectonic contacts by an unconformity at the base Middle Miocene (Tischler *et al.* 2006). This truncation could either be explained by exhumation by erosion in the internal part of an accretionary wedge or by exhumation which postdates nappe emplacement.

Regarding the age and the amounts of exhumation, our data are generally in good accordance with earlier apatite FT data (Sanders 1998; Sanders *et al.* 1999; see Fig. 12). However, in contrast to Sanders (1998), our data indicate full annealing of apatite in all the basement units of the Bucovinian nappe stack. Hence we infer slightly higher values of exhumation.

Relationships between uplift and cooling

The age vs. altitude relation (Fig. 11) indicates fast exhumation between 12 and 11 Ma in the Rodna horst, contemporaneous with the stratigraphically dated tectonic transtensional stage (12 to 10 Ma). On the other hand, thermal modelling of FT data indicates fast cooling between 11 and 7 Ma, i.e. slightly later. However, given high exhumation rates, the observed cooling history of a sample is not only influenced by the exhumation rate alone (Brown 1991; Mancktelow & Grasemann 1997). Starting at rates exceeding 1 mm/a, advective heat transport will cause a delay of cooling with respect to exhumation (Mancktelow & Grasemann 1997). Advective heat transport not only causes a decrease in the spacing of the isotherms (i.e. an increase in geothermal gradient) but can also lead to formation of non-planar isotherms in areas with rugged relief (Stüwe *et al*. 1994; Mancktelow & Grasemann 1997; Braun 2002). Following these authors, we interpret the delay between fast exhumation and fast cooling, as documented by Middle to Late Miocene cooling ages, as an effect of advective heat transport during a limited phase of fast tectonic exhumation. Sanders (1998) determined mean erosion rates of 0.5 mm/a in the East Carpathians for about the same time interval, i.e. from Middle Miocene to Pliocene times (15 to 5 Ma).

Uplift and exhumation at a regional scale

Middle Miocene ages in the western part of the study area reflect a first stage of exhumation related to the transpressional stage of deformation. The stratigraphically dated Middle Miocene transpressional stage (16 to 12 Ma) is interpreted as a result of the NE-directed perpendicular convergence during soft collision of Tisza–Dacia with the NW–SE striking European margin.

The enhanced Middle to Late Miocene exhumation rates deduced from thermochronological analyses are contemporaneous with the transtensional stage of deformation documented in the study area. The transtensional stage of deformation is thought to be the result of oblique convergence of Tisza–Dacia with the NW–SE striking European margin, evidenced by eastward thrusting in the external Miocene thrust belt (Matenco & Bertotti 2000). Blocking of eastward movement of Tisza–Dacia in the north led to sinistral strike-slip activity along E–W trending faults and coeval normal faulting along NE–SW directed faults (Tischler *et al.* 2006). This fragmentation of the crust by normal and sinistral strike-slip faulting into SW down-tilted blocks led to the development of triangle-shaped graben (Borsa graben) and corresponding horst structures (Rodna horst; Fig. 12). Exhumation of internal units during foreland propagating thrusting is also known from the westernmost Carpathians. Danišík *et al.* (2004) report enhanced Middle Miocene exhumation in the northern Danube basin, documented by apatite FT ages (16 to 13 Ma), contemporaneous with north-directed emplacement and thrusting in the Miocene thrust belt further to the N (16 to 14 Ma, e.g. Jiricek 1979).

Although the main activity of the Bogdan–Dragos–Voda fault system terminated at 10 Ma, extensional veins within the volcanic body of Baia Mare, featuring hydrothermal ore deposits (7 to 8 Ma, Lang *et al.* 1994), suggest minor extensional activity after 10 Ma. Possible Late Miocene normal and strike-slip faulting may explain the extraordinarily young apatite FT ages (7.8 Ma, Fig. 12) in the SE part of the study area. Such a Late Miocene exhumation would be contemporaneous with strike-slip deformation in the external East Carpathian Miocene thrust belt, dated at 9 Ma (Matenco & Bertotti 2000).

Conclusions

The basement units of the Maramures Mountains, the Rodna horst and the Preluca massif suffered a last stage of metamorphism under sub-greenschist to lowermost greenschist facies conditions during the later Early Cretaceous, followed by Late Cretaceous cooling and exhumation. Palaeogene to Early Miocene sedimentation and thrusting caused renewed heating by burial, which led to full annealing of fission tracks in apatite in parts of the study area.

Soft collision of Tisza–Dacia with the European margin initiated a first transpressional tectonic stage (16 to 12 Ma) which caused exhumation by folding and reverse faulting in the western part of the study area. Middle Miocene cooling ages (15.0 to 13.2 Ma) are related to this tectonic stage.

Transpression was followed by transtension (12 to 10 Ma) during ongoing NE–SW shortening. The late-stage evolution of the Rodna horst is dominated by combined normal and strike-slip faulting, which led to its fragmentation into tilted and fault-bounded blocks. Fast exhumation in the central part of the Rodna area resulted in Middle to Late Miocene cooling ages (12.7 to 7.3 Ma). Exhumation rates exceeded 1 mm/a during this stage and caused advective heat transport leading to delayed cooling.

We are most grateful for the excellent introduction into the study area and its geology provided by M. Săndulescu and L. Matenco and their ongoing support. L. Matenco also critically reviewed a first version of the manuscript. Fruitful discussions with D. Badescu, M. Marin, I. Balintoni and D. Radu are also highly appreciated. H.R.G. is very grateful to F. Stuart for his introduction to the lab. procedures and methods of (U–Th)/He analysis. Furthermore, we thank I. Dunkl and M. Raab for their careful reviews and constructive remarks. Financial support by the Swiss National Science foundation (NF-project Nr. 21-64979.01, granted to B.F.) is gratefully acknowledged.

References

Andriessen, P. A. M. 1995. Fission track analysis: principles, methodology, and implications for tectono-thermal histories of sediment basins, orogenic belts and continental margins. *Geologie en Mijnbouw*, **74**, 1–12.

Aroldi, C. 2001. *The Pienides in Maramures—Sedimentation, Tectonics and Paleogeography*. Cluj, PhD thesis, Universitaria Babes—Bolyai Cluj.

Balestrieri, M. L., Stuart, F. M., Persano, C., Abbate, E. & Bigazzi, G. 2005. Geomorphic development of the escarpment of the Eritrean margin, southern Red Sea from combined apatite fission-track and (U–Th)/He thermochronometry. *Earth and Planetary Science Letters*, **231**, 97–110.

Balintoni, I., Mosonyi, E. & Puste, A. 1997. Informatii si interpretari litostratigrafice, metamorfice si structurale privitoare la masivul Rodna (Carpatii orientali). *Studia Universitates Babes—Bolyai*. **Geologia XLII**, 51–66.

Balla, Z. 1987. Tertiary paleomagnetic data for the Carpatho-Pannonian region in the light of Miocene rotation kinematics. *Tectonophysics*, **139**, 67–98.

Borcos, M., Sandulescu, M., Stan, N., Peltz, S., Marinescu, F. & Ticleanu, N. 1980. *Geological Map 1:50 000 Cavnic*. Institutul de Geologie şi Geofizica, Bucharest.

Braun, J. 2002. Quantifying the effect of recent relief changes on age-elevation relationships. *Earth and Planetary Science Letters*, **200**, 331–343.

Broucker, G. de, Mellin, A. & Duindam, P. 1998. Tectonostratigraphic evolution of the Transylvanian Basin, Pre-Salt sequence, Romania. *In*: Dinu, C. (ed.) *Bucharest Geoscience Forum.* Special volume, **1**, 36–70.

Brown, R. W. 1991. Backstacking apatite fission track 'stratigraphy': a method for resolving the erosional and isostatic rebound components of tectonic uplift histories. *Geology*, **19**, 74–77.

Burtner, R. L., Nigrini, A. & Donelick, R. A. 1994. Thermochronology of the Lower Cretaceous source rocks in the Idaho-Wyoming thrust belt. *AAPG Bulletin*, **78**, 1613–1636.

Ciulavu, D., Dinu, C. & Cloetingh, S. A. P. L. 2002. Late Cenozoic tectonic evolution of the Transylvanian basin and north-eastern part of the Pannonian basin (Romania): constraints from seismic profiling and numerical modeling. *EGU Stephan Mueller Special Publication Series*, **3**, 105–120.

Crowley, K. D. 1985. Thermal significance of fission-track length distributions. *Nuclear Tracks*, **10**, 311–322.

Crowley, K. D. & Cameron, M. 1987. Annealing of etchable fission-track damage in apatite: effects of anion chemistry. *Geological Society of America Abstract Program*, **19**, 631–632.

Csontos, L. 1995. Tertiary tectonic evolution of the Intra-Carpathian area: a review. *Acta Vulcanologica*, **7**, 1–13.

Csontos, L. & Nagymarosy, A. 1998. The Mid-Hungarian line: a zone of repeated tectonic inversions. *Tectonophysics*, **297**, 51–71.

Csontos, L. & Vörös, A. 2004. Mesozoic plate tectonic reconstruction of the Carpathian region. *Palaeocgeography, Palaeoclimatology, Palaeoecology*, **210**, 1–56.

Csontos, L., Nagymarosy, A., Horváth, F. & Kováč, M. 1992. Cenozoic evolution of the Intra-Carpathian area: a model. *Tectonophysics*, **208**, 221–241.

Danišík, M., Dunkl, I., Putis, M., Frisch, W. & Kral, J. 2004. Tertiary burial and exhumation history of basement highs along the NW margin of the Pannonian basin an apatite fission track study. *Austrian Journal of Earth Sciences*, **95/96**, 60–70.

Demetrescu, C. & Veliciu, S. 1991. Heat flow and lithosphere structure in Romania. *In*: Cermak, V. & Rybach, L. (eds) *Terrestrial Heat Flow and the Lithosphere Structure.* Springer-Verlag, Berlin, New York, 187–205.

DICEA, O., DUTESCU, P., ANTONESCU, F. *ET AL*. 1980. Contributii la cunoasterea stratigrafiei zonei transcarpatice din maramures. *Dari de Seama Institutul Geologie şi Geofizica*, **LXV**, 21–85.

DUMITRU, T. 1993. A new computer-automated microscope stage system for fission-track analysis. *Nuclear Tracks and Radiation Measurements*, **21**, 575–580.

DUNKL, I. 2002. TrackKey: a Windows program for calculation and graphical presentation of fission track data. *Computers & Geosciences*, **28**, 3–12.

DUNKL, I. & FRISCH, W. 2002. Thermochronological constraints on the Late Cenozoic exhumation along the Alpine and Western Carpathian margins of the Pannonian basin. *EGU Stephan Mueller Special Publications Series*, **3**, 135–147.

DUNKL, I. & SZÉKELY, B. 2002. Component analysis with visualization of fitting PopShare, a Windows program for data analysis. Goldschmidt Conference Abstracts 2002. *Geochimica et Cosmochimica Acta*, **66/15A**, 201.

EHLERS, T. A. & FARLEY, K. A. 2003. Apatite (U–Th)/He thermochronometry: methods and applications to problems in tectonic and surface processes. *Earth and Planetary Science Letters*, **206**, 1–14.

FARLEY, K. A. 2000. Helium diffusion from apatite: general behaviour as illustrated by Durango fluorapatite. *Journal of Geophysical Research*, **105**, 2903–2914.

FARLEY, K. A. 2002. (U/Th)/He dating: techniques, calibrations, and applications. *In*: PORCELLI, P. D., BALLENTINE, C. J. & WIELER, R. (eds) *Noble Gas Geochemistry*. Reviews in Minerology and Geochemistry, **47**, 819–843.

FODOR, L., CSONTOS, L., BADA, G., GYÖRFI, I. & BENKOVICS, L. 1999. Tertiary tectonic evolution of the Pannonian Basin system and neighbouring orogens: a new synthesis of paleostress data. *In*: DURAND, B., JOLIVET, L., HORVÁTH, E. & SÉRANNE, M. (eds) *The Mediterranean Basins: Tertiary Extension within the Alpine Orogen*. London, Geological Society, **156**, 295–334.

FOEKEN, J. P. T., DUNAI, T. J., BETOTTI, G. & ANDRIESSEN, P. A. M. 2003. Late Miocene to present exhumation in the Ligurian Alps (southwest Alps) with evidence for accelerated denudation during the Messinian salinity crisis. *Geology*, **31**, 797–800.

FOEKEN, J. P. T., STUART, F. M., DOBSON, K. J., PERSANO, C. & VILBERT, D. 2006. A diode laser system for heating minerals for (U–Th)/He chronometry. *Geochemistry Geophysics and Geosystems*, **7**, Q04015, doi: 10.1029/2005GC001190.

FÜGENSCHUH, B. & SCHMID, S. M. 2003. Late stages of deformation and exhumation of an orogen constrained by fission-track data: a case study in the Western Alps. *GSA Bulletin*, **115**, 1425–1440.

FÜGENSCHUH, B. & SCHMID, S. M. 2005. Age and significance of core complex formation in a highly bent orogen: evidence from fission track studies in the South Carpathians (Romania). *Tectonophysics*, **404**, 33–35.

FÜGENSCHUH, B., MANCKTELOW, N. S. & SEWARD, D. 2000. Cretaceous to Neogene cooling and exhumation history of the Oetztal-Stubai basement complex, Eastern Alps: a structural and fission track study. *Tectonics*, **19**, 905–918.

GALBRAITH, R. F. 1981. On statistical models for fission track counts. *Mathematical Geology*, **13**, 471–478.

GALBRAITH, R. F. 1990. The radial plot: graphical assessment of spread in ages. *Nuclear Tracks in Radiation Measurements*, **17**, 207–214.

GALBRAITH, R. F. & LASLETT, G. M. 1993. Statistical models for mixed fission track ages. *Nuclear Tracks in Radiation Measurements*, **21**, 459–470.

GALLAGHER, K., BROWN, R. & JOHNSON, C. 1998. Fission track analysis and its applications to geological problems. *Annual Reviews in Earth and Planetary Science Letters*, **26**, 519–571.

GIUSCA, D. & RADULESCU, D. 1967. *Geological Map 1:200 000 Baia Mare*. Institutul de Geologie şi Geofizica, Bucharest.

GLEADOW, A. J. W. 1981. Fission-track dating methods: what are the real alternatives? *Nuclear Tracks*, **5**, 3–14.

GLEADOW, A. J. W. & DUDDY, I. R. 1981. A natural long-term track annealing experiment for apatite. *Nuclear Tracks*, **5**, 169–174.

GLEADOW, A. J. W., DUDDY, I. R., GREEN, P. F. & LOVERING, J. F. 1986*a*. Confined track lengths in apatite: a diagnostic tool for thermal history analysis. *Contributions to Mineralogy and Petrology*, **94**, 405–415.

GLEADOW, A. J. W., DUDDY, I. R., GREEN, P. F. & HEGARTY, K. A. 1986*b*. Fission track lengths in the apatite annealing zone and the interpretation of mixed ages. *Earth and Planetary Science Letters*, **78**, 245–254.

GRADSTEIN, F., OGG, J. & SMITH, A. 2004. *A Geologic Time Scale*. Cambridge University Press, Cambridge.

GREEN, P. F., DUDDY, I. R., GLEADOW, A. J. W. & TINGATE, P. R. 1985. Fission track annealing in apatite: Track length measurements and the form of the Arrhenius plot. *Nuclear Tracks*, **10**, 323–328.

GREEN, P. F., DUDDY, I. R., GLEADOW, A. J. W., TINGATE, P. R. & LASLETT, G. M. 1986. Thermal annealing of fission tracks in apatite, 1. A qualitative description. *Chemical Geology*, **59**, 237–253.

GREEN, P. F., DUDDY, I. R., LASLETT, G. M., HEGARTY, K. A., GLEADOW, A. J. W. & LOVERING, J. F. 1989. Thermal annealing of fission tracks in apatite, 4. Quantitative modelling techniques and extension to geological timecales. *Chemical Geology*, **79**, 155–182.

HAAS, J. & PÉRÓ, S. 2004. Mesozoic evolution of the Tisza Mega-unit. *International Journal of Earth Science*, **93**, 297–313.

HOUSE, M. A., FARLEY, K. A. & STÖCKLI, D. F. 2000. Helium chronometry of apatite and titanite using Nd: YAG laser heating. *Earth and Planetary Science Letters*, **183**, 365–368.

HURFORD, A. J. 1986. Cooling and uplift patterns in the Lepontine Alps South Central Switzerland and an age of vertical movement on the Insubric fault line. *Contributions to Mineralogy and Petrology*, **92**, 413–427.

HURFORD, A. J. & GREEN, P. F. 1983. The zeta age calibration of fission-track dating. *Isotope Geoscience*, **1**, 285–317.

IANOVICI, V. & DESSILA-CODARCEA, M. 1968. *Geological Map 1:200 000 Radauti*. Institutul de Geologie şi Geofizica, Bucharest.

IANOVICI, V. & RADULESCU, D. 1968. *Geological Map 1:200 000 Toplita*. Institutul de Geologie şi Geofizica, Bucharest.

IANOVICI, V., RADULESCU, D. & PATRULIUS, D. 1968. *Geological Map 1:200 000 Viseu*. Institutul de Geologie şi Geofizica, Bucharest.

JIRICEK, R. 1979. Tectonic development of the Capathian arc in the Oligocene and Neogene. *In*: MAHEL, M. (ed.) *Tectonic Profiles Through the Western Carpathians*. Geological Institute Dionyz Stur, Bratislava, 205–214.

KETCHAM, R. A., DONELICK, R. A., & DONELICK, M. B. 2000. AFTSolve: a program for multi-kinetic modeling of apatite fission-track data. *Geological Materials Research*, **2**, (electronic).

KRÄUTNER, H. G. 1991. Pre-Alpine geological evolution of the East Carpathian metamorphics. Some common trends with the West Carpathians. *Geologica Carpathica*, **42**, 209–217.

KRÄUTNER, H. G., KRÄUTNER, F., SZASZ, L., UDUBASA, G. & ISTRATE, G. 1978. *Geological Map 1:50 000 Rodna Veche*. Institutul de Geologie şi Geofizica, Bucharest.

KRÄUTNER, H. G., KRÄUTNER, F. & SZASZ, L. 1982. *Geological Map 1:50 000 Pietrosul Rodnei*. Institutul de Geologie şi Geofizica, Bucharest.

KRÄUTNER, H. G., KRÄUTNER, F. & SZASZ, L. 1983. *Geological Map 1:50 000 Ineu*. Institutul de Geologie şi Geofizica, Bucharest.

KRÄUTNER, H. G., KRÄUTNER, F., SZASZ, L. & SEGHEDI, I. 1989. *Geological Map 1:50 000 Rebra*. Institutul de Geologie şi Geofizica, Bucharest.

LANG, B., EDELSTEIN, O., STEINITS, G., KOVACS, M. & HALGA, S. 1994. Ar-Ar dating of adulari—a tool in understanding genetic relations between volcanism and mineralization: Baia Mare (Gutii Mountains), northwestern Romania. *Economic Geology*, **89**, 174–180.

LASLETT, G. M., GREEN, P. F., DUDDY, I. R. & GLEADOW, A. J. W. 1987. Thermal annealing of fission tracks in apatite, 1. A quantitative analysis. *Chemical Geology*, **65**, 1–13.

MANCKTELOW, N. S. & GRASEMANN, B. 1997. Time-dependent effects of heat advection and topography on cooling histories during erosion. *Tectonophysics*, **270**, 167–195.

MÁRTON, E. 2000. The Tisza Megatectonic Unit in the light of paleomagnetic data. *Acta Geologica Hungary*, **43**, 329–343.

MÁRTON, E. & FODOR, L. 1995. Combination of palaeomagnetic and stress data—a case study from North Hungary. *Tectonophysics*, **242**, 99–114.

MÁRTON, E. & FODOR, L. 2003. Tertiary paleomagnetic results and structural analysis from the Transdanubian Range (Hungary): rotational disintegration of the ALCAPA unit. *Tectonophysics*, **363**, 201–224.

MÁRTON, E., TISCHLER, M., CSONTOS, L., FÜGENSCHUH, B. & SCHMID, S. M. 2006. The contact zone between the ALCAPA and Tisza–Dacia mega-tectonic units of Northern Romania in the light of new paleomagnetic data. *Swiss Journal of Geoscience*, **100**, 109–124.

MASON, P. R. D., SEGHEDI, I., SZAKASC, A. & DOWNES, H. 1998. Magmatic constraints on geodynamic models of subduction in the Eastern Carpathians, Romania. *Tectonophysics*, **297**, 157–176.

MATENCO, L. & BERTOTTI, G. 2000. Tertiary tectonic evolution of the external East Carpathians (Romania). *Tectonophysics*, **316**, 255–286.

MORLEY, C. K. 2002. Tectonic settings of continental extensional provinces and their impact on sedimentation and hydrocarbon prospectivity. *In*: RENAUT, R. W. & ASHLEY, G. M. (eds) *Sedimentation in Continental Rifts*. Society of Sedimentary Geology, Special publications, **73**, 25–55.

ÒSULLIVAN, P. B. & PARRISH, R. R. 1995. The importance of apatite composition and single-grain ages when interpreting fission track data from plutonic rocks: a case study from the Coast Ranges, British Columbia. *Earth and Planetary Science Letters*, **132**, 213–224.

PÉCSKAY, Z., EDELSTEIN, O., SEGHEDI, I., SZAKÁCS, A., KOVACS, M., CRIHAN, M. & BERNÁD, A. 1995. K-Ar datings of Neogene-Quaternary calc-alkaline volcanic rocks in Romania. *In*: DOWNES, H. & VASELLI, O. (eds) Neogene and related magmatism in the Carpatho-Pannonian Region. *Acta Vulcanologica*, **7**, 53–61.

PERSANO, C., STUART, F. M., BISHOP, P. & DEMPSTER, T. J. 2005. Deciphering continental breakup in eastern Australia using low temperature thermochronometers. *Journal of Geophysical Research*, **110**, doi: 10.1029/2004JB003325.

RAILEANU, G. & RADULESCU, D. 1967. *Geological Map 1:200 000 Bistrita*. Institutul de Geologie şi Geofizica, Bucharest.

RAILEANU, G. & SAULEA, E. 1968. *Geological Map 1:200 000 Cluj*. Institutul de Geologie şi Geofizica, Bucharest.

RATSCHBACHER, L., MERLE, O., DAVY, P. & COBBOLD, P. 1991*a*. Lateral extrusion in the Eastern Alps; Part 1, Boundary conditions and experiments scaled for gravity. *Tectonics*, **10**, 245–256.

RATSCHBACHER, L., FRISCH, W., LINZER, H. G. & MERLE, O. 1991*b*. Lateral extrusion in the Eastern Alps; Part 2, Structural analysis. *Tectonics*, **10**, 257–271.

REINERS, P. W. & EHLERS, T. A. (eds) 2005. Low-temperature thermochronology: techniques, interpretations, and applications. *Reviews in Mineralogy and Geochemistry*, **58**.

REINERS, P. W., ZHOU, Z., EHLERS, T., XU, C., BRANDON, M. T., DONELICK, R. A. & NICOLESCU, S. 2003. Post-orogenic evolution of the Dabie Shan, eastern China, from (U–Th)/He and fission track thermochronology. *American Journal of Science*, **303**, 489–518.

ROURE, F., BESSEREAU, G., KOTARBA, M., KUSMIEREK, J. & STRZETELSKI, W. 1993. Structure and hydrocarbon habitats of the Polish Carpathian Province. *American Association of Petroleum Geologists Bulletin*, **77**, 1660.

ROYDEN, L. H. 1988. Late Cenozoic Tectonics of the Pannonian Basin System. *In*: ROYDON, L. H. & HORVÁTH, F. (eds) *The Pannonian Basin: A Study In Basin Evolution*. Tulsa, Oklahoma, The American Association of Petroleum Geologists, **45**, 27–48.

ROYDEN, L. H. 1993. The tectonic expression of slab pull at continental convergent boundaries. *Tectonics*, **12**, 303–325.

ROYDEN, L. H. & BÁLDI, T. 1988. Early Cenozoic tectonics and paleogeography of the Pannonian and surounding regions. *In*: ROYDON, L. H. & HORVÁTH, F. (eds) *The Pannonian Basin: A Study In Basin Evolution.* Tulsa, Oklahoma, The American Association of Petroleum Geologists, **45**, 1–16.

RUSU, A., BALINTONI, I., BOMBITA, G. & POPESCU, G. 1983. *Geological Map 1:50 000 Preluca*. Institutul de Geologie şi Geofizica, Bucharest.

SANDERS, C. 1998. *Tectonics and Erosion-Competitive Forces in a Compressive Orogen: A Fission Track Study of the Romanian Carpathians.* PhD thesis, Vrije Universiteit Amsterdam, 1–204.

SANDERS, C. A. E., ANDRIESSEN, P. A. M. & CLOETINGH, S. A. P. L. 1999. Life cycle of the East Carpathian orogen: erosion history of a double vergent critical wedge assessed by fission track thermochronology. *Journal of Geophysical Research*, **104**, 29095–29112.

SĂNDULESCU, M. 1980. Sur certain problèmes de la corrélation des Carpathes orientales Roumaines avec les Carpathes Ucrainiennes. *Dari de Seama Institutul Geologie şi Geofizica*, **LXV**, 163–180.

SĂNDULESCU, M. 1982. Contributions à la connaissance de nappes Crétacées de Monts du Maramures (Carpathes Orientales). *Dari de Seama Institutul Geologie şi Geofizica*, **LXIX**, 83–96.

SĂNDULESCU, M. 1988. Cenozoic Tectonic History of the Carpathians. *In*: ROYDEN, L. H. & HORVÁTH, F. (eds) *The Pannonian Basin; a study in basin evolution.* Tulsa, Oklahoma, The American Association of Petroleum Geologists, **45**, 17–26.

SĂNDULESCU, M. 1994. Overview on Romanian Geology. *In*: 2nd Alcapa Congress, Field guidebook, *Romanian Journal of Tectonics and Regional Geology*, **75**, 3–15.

SĂNDULESCU, M. & RUSSO-SĂNDULESCU, D. 1981. *Geological Map 1:50 000 Poiana Botizii*. Institutul de Geologie şi Geofizica, Bucharest.

SĂNDULESCU, M., KRÄUTNER, H. G., BALINTONI, I., RUSSO-SĂNDULESCU, D. & MICU, M. 1981. *The Structure of the East Carpathians, (Guide Book B1).* Carpathian Balkan Geological Association, 12th Congress, Bucharest.

SĂNDULESCU, M., SZASZ, L., BALINTONI, I., RUSSO-SĂNDULESCU, D. & BADESCU, D. 1991. *Geological Map 1:50 000 No 8d Viseu*. Institutul de Geologie şi Geofizica, Bucharest.

SĂNDULESCU, M., VISARION, M., STANICA, D., STANICA, M. & ATANASIU, L. 1993. Deep structure of the inner Carpathians in the Maramures-Tisa zone (East Carpathians). *Romanian Journal of Geophysics*, **16**, 67–76.

SCHMID, S. M., FÜGENSCHUH, B., MATENCO, L., SCHUSTER, R., TISCHLER, M. & USTASZEWSKI, K. 2006. The Alps-Carpathians-Dinarides-connection: a compilation of tectonic units. 18th Congress of the Carpathian-Balkan Geological Association, Belgrade, Serbia, Sept. 3–6, 2006. *Conference Proceedings*, 535–538.

SIDDALL, R. & HURFORD, A. J. 1998. Semi-quantitative determination of apatite anion composition for fission-track analysis using infra-red microspectroscopy. *Chemical Geology*, **150**, 181–190.

SOBEL, E. R. & DUMITRU, T. A. 1997. Thrusting and exhumation around the margins of the western Tarim basin during the India-Asia collision. *Journal of Geophysical Research*, **102**, 5043–5063.

SPERNER, B., CRC 461 TEAM 2005. Monitoring of Slab Detachment in the Carpathians. *In*: WENZEL, F. (ed.) Perspectives in modern seismology. *Lecture Notes in Earth Sciences*, **105**, 187–202.

STEININGER, F. F. & WESSELY, G. 2000. From the Tethyan ocean to the Paratethys Sea: Olicocene to Neogene stratigraphy, paleogeography and paleobiogeography of the circum-Mediterranean region and the Oligocene to Neogene basin evolution in Austria. *Mitteilungen der Österreichischen Geologischen Gesellschaft*, **92**, 95–116.

STÖCKLI, D. F. 2005. Application of low-temperature thermochronometry to extensional tectonic settings. *In*: REINERS, P. W. & EHLERS, T. A. (eds) *Low-Temperature Thermochronology: Techniques, Interpretations, and Applications. Reviews in Mineralogy and Geochemistry*, **58**, 411–448.

STÜWE, K., WHITE, L. & BROWN, R. 1994. The influence of eroding topography on steady-state isotherms. Applications to fission-track analysis. *Earth and Planetary Sciene Letters*, **124**, 63–74.

TISCHLER, M., GRÖGER, H. R., FÜGENSCHUH, B. & SCHMID, S. M. 2006. Miocene tectonics of the Maramures area (Northern Romania)—implications for the Mid-Hungarian fault zone. doi: 10.1007/s00531-006-0110-x. *International Journal of Earth Sciences*, **96**, 473–496.

TISCHLER, M., MATENCO, L., FILIPESCU, S., GRÖGER, H. R., WETZEL, A. & FÜGENSCHUH, B. 2008. Tectonics and sedimentation during convergence of the ALCAPA and Tisza–Dacia: continental blocks the Pienide nappe emplacement and its foredeep (N. Romania) *In*: SIEGESMUND, S., FÜGENSCHUH, B. & FROITZHEIM, N. (eds) *Tectonic Aspects of the Alpine-Dinaride-Carpathian Systems*, **298**, 317–334.

VELICIU, S. & VISARION, M. 1984. Geothermal models for the East Carpathians. *Tectonophysics*, **103**, 157–165.

VODA, A. & BALINTONI, I. 1994. Corelari lithostratigrafice în cristalinul Carpatilor Orientali. *Studia Universitates Babes—Bolyai*, *Geologia*, **XXXIX**, 61–66.

WAGNER, G. A. & VAN DEN HAUTE, P. 1992. *Fission-Track Dating*. Stuttgart, Enke Verlag.

WOLF, R. A., FARLEY, K. A. & KASS, D. M. 1998. Modeling of the temperature sensitivity of the apatite (U–Th)/He thermochronometer. *Chemical Geology*, **148**, 105–114.

WORTEL, M. J. R. & SPAKMAN, W. 2000. Subduction and slab detachment in the Mediterranean-Carpathian region. *Science*, **290**, 1910–1917.

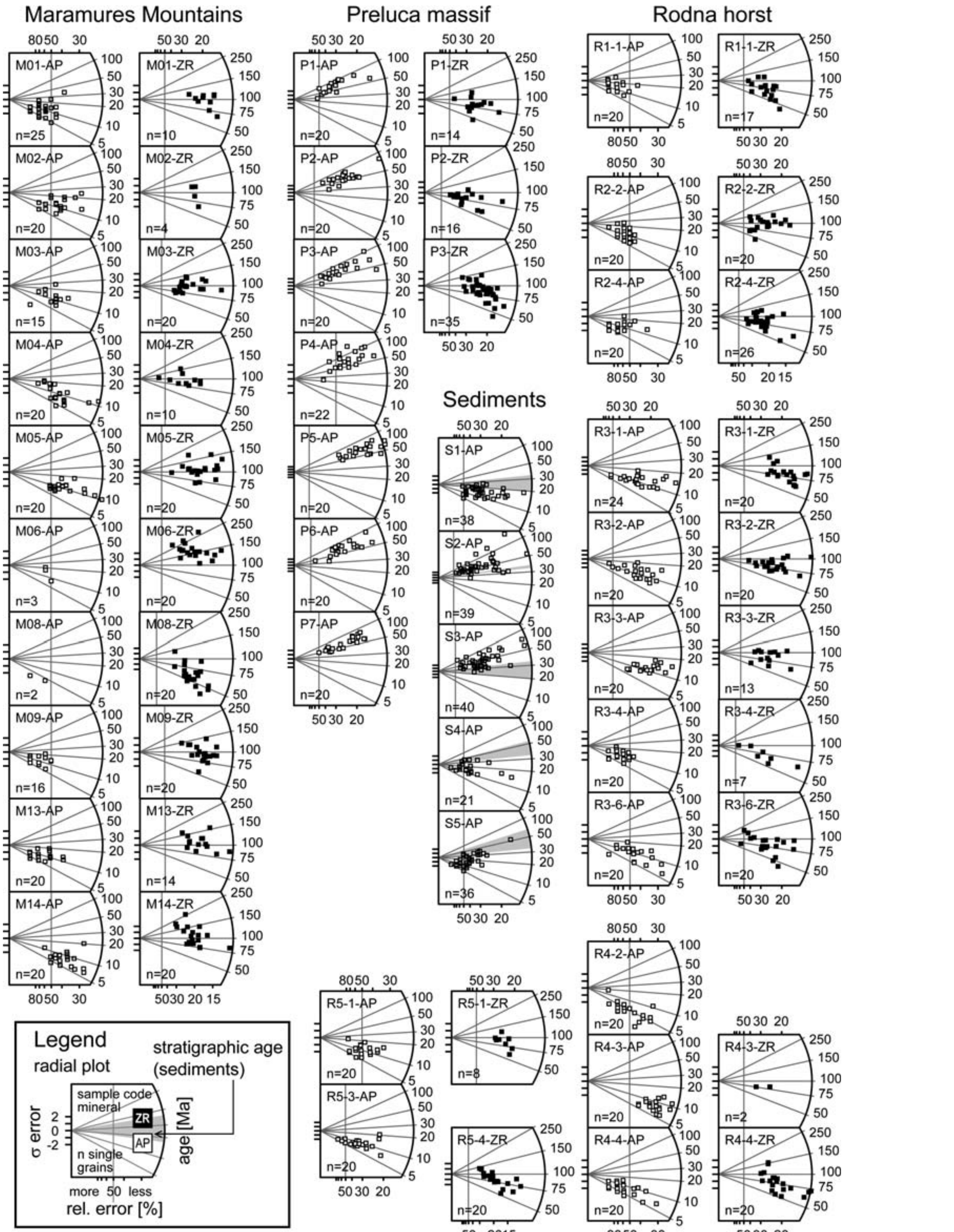

Appendix 1a. Results of fission track analyses in the study area: radial plots. All radial plots (Galbraith 1990) of the same data group (Ap/Zr) show the same age spectrum to allow for direct comparison.

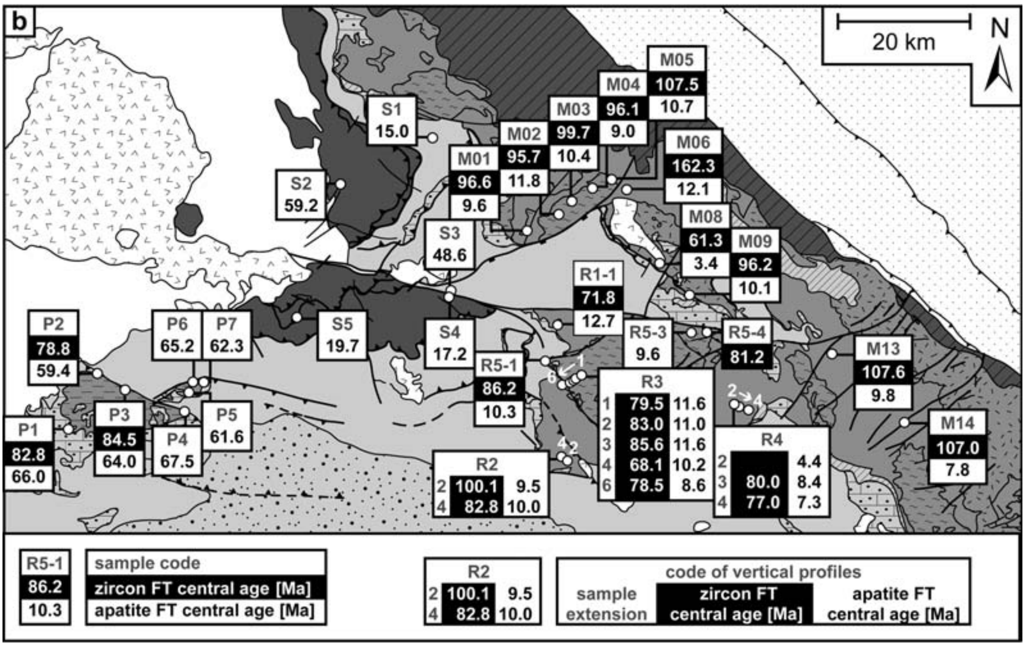

Appendix 1b. Results of fission track analyses in the study area: ages in map view. All given ages in the map are central ages (Galbraith & Laslett 1993).

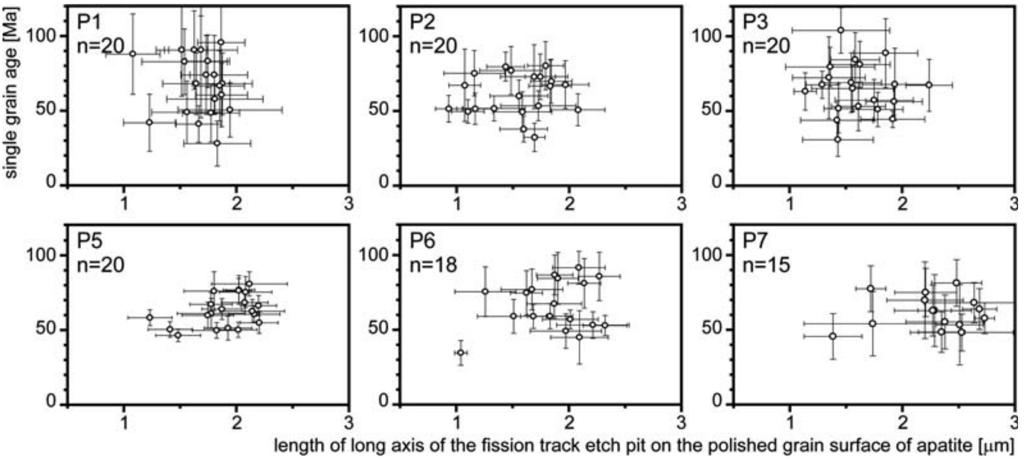

Appendix 2. Etch pit long axes measurements of the samples from the Preluca massif. P4 did not provide enough spontaneous tracks. Generally, as many as possible etch pit long axes per grain were measured, up to a maximum of ten. The grain ages are plotted with their single grain error and the mean of the etch pit long axes is plotted with one standard deviation.